VALIDATION AND INSIGHT INTO A NOVEL PACKED-BED ELECTRODE FLOW BATTERY ARCHITECTURE

A Dissertation presented to the Faculty of the Graduate School

University of Missouri

In Partial Fulfillment

Of the Requirements for the Degree

Doctor of Philosophy

---

by

BRYAN DUSTIN SAWYER

Dr. Galen Suppes, Dissertation Supervisor

DECEMBER 2010

The undersigned, appointed by the Dean of the Graduate School, have examined the dissertation entitled

VALIDATION AND INSIGHT INTO A NOVEL PACKED-BED ELECTRODE FLOW BATTERY ARCHITECTURE

Presented by Bryan D. Sawyer

A candidate for the degree of Doctor of Philosophy

And hereby certify that in their opinion it is worthy of acceptance.

_____

Dr. Galen J. Suppes

_____

Dr. Thomas R. Marrero

_____

Dr. Truman S. Storvick

_____

Dr. John M. Gahl

DEDICATION

This dissertation is dedicated to my parents, Hugh B. Sawyer and Brenda J. Sawyer, for their continuous love, support, and encouragement throughout all of my lifelong endeavors. Despite tough financial times, their supplemental financial support and sacrifice made my undergraduate education possible. Without this important pedestal my graduate education could not have been possible.

ACKNOWLEDGEMENTS

My deepest gratitude is extended to my dissertation supervisor, Dr. Galen J. Suppes, for the opportunity to pursue energy related graduate studies. With the changed landscape of our research group, it is his enthusiasm, foresight, instruction, and positive attitude that have provided encouragement to pursue new concepts related to electrical energy storage and to think beyond the current electrical energy storage paradigms. His professionalism has been a great example and his friendship has been much appreciated.

I would also like to extend deep gratitude to the rest of my doctoral dissertation committee members; Dr. Thomas R. Marrero, Dr. Truman S. Storvick, and Dr. John M. Gahl for their valuable time, constructive criticisms, suggestions, and evaluations throughout my dissertation process. It is truly an honor to have such distinguished and decorated professionals as members of my committee.

Much gratitude is extended to my graduate research colleagues; Michael Gordon and Eric Leimkuehler, for their assistance and for providing an entertaining work environment. I would also like to say thank you to my undergraduate research colleagues; Matthias Young, Matt Wavada, and Michael Heidlage for their positive contributions to the research group and for their cooperation in scheduling lab equipment use. Special thanks goes to research specialist Ali Tekeei who was always willing to provide an extra set of hands or great advice.

I also wish to thank the department secretary Rita Preckshot for her assistance in the ordering and procuring supplies and equipment, her witty humor, and the tasty treats she often provided the department. Thanks also to the department administrative assistant Stacy Bono for her assistance in the ordering and procuring of supplies and equipment and for the smooth handling of the administrative paperwork on my behalf.

I would also like to thank members of Engineering Technical Services team; Michael Klote, Richard Oberto, and Michael Absheer for their excellent technical help with electronics and National Instruments LabVIEW programming, not only on my personal projects, but also on College of Engineering and Department of Chemical Engineering endeavors. A special thanks also to Brian Samuels for his top-notch instruction and help in the machine shop.

I would especially like to thank the National Science Foundation for the financial support of my research that is reported in this dissertation (Award 0940720).

TABLE OF CONTENTS

LIST OF ILLUSTRATIONS

List of Tables

List of Figures

VALIDATION AND INSIGHT INTO A NOVEL PACKED-BED ELECTRODE FLOW BATTERY ARCHITECTURE

Bryan D. Sawyer

Dr. Galen J. Suppes, Dissertation Supervisor

ABSTRACT

Large-scale electrical energy storage devices are important for efficiently using existing power generation infrastructure, provide stability to renewable power generation, and displacing liquid fossil fuel use in the transportation sector. This project proposes a novel flow battery architecture that employs packed-beds of granular active materials as positive and negative electrodes. This design is expected to improve upon existing battery technologies and most importantly to increase the specific energy of flow battery technology to extend their use to vehicle applications.

This research validates the use of packed-bed electrodes in a flow battery configuration and determines the effects of electrode separation distance, stationary versus flowing electrolyte, ionically active electrode separation materials, separation distance using separation materials, and the direction of electrolyte circulation. These are fundamental parameters that must be determined to provide a packed-bed electrode flow battery (PBEFB) configuration to be used for continued development of the technology.

Zinc/alkaline/manganese dioxide battery chemistry was applied to the PBEFB design for all investigations presented in this dissertation. Two PBEFB configurations were used in these investigations: 1) 2-stainless steel cylinders with stainless steel piston tops (active material containment and current collection) were connected with non-conductive peristaltic pump hose , and 2) 2-stainless steel tubes (active material containment and current collection) were stacked vertically and connected by a non-conductive high-density polyethylene coupling. Overpotentials were revealed using voltage-time profiles and were used as the basis for performance discussions throughout this research. In all experiments, a 550-ohm load was used to discharge the PBEFB to obtain the voltage-time curves.

The effect of electrolyte flow was studied using the second PBEFB configuration. During discharge the PBEFB was subjected to 20-minutes of electrolyte flow, subsequent 20-minutes without electrolyte flow, and then final subsequent 20-minutes of electrolyte flow. This investigation was completed with 3 different electrolyte configurations; 2, 3, and 4 molar potassium hydroxide solutions. The results indicated that without electrolyte flow an increase in overpotential occurs and that higher concentration electrolytes exhibit less overpotential increase with a lack of electrolyte flow. The re-establishment of electrolyte flow immediately reduced the overpotentials associated with the lack of electrolyte flow and voltage profiles returned to similar discharge slopes as those seen prior to stopping electrolyte flow.

Electrode separation distance was investigated using the first PBEFB configuration. Varied lengths of peristaltic pump hose were used to determine the overpotentials associated with changing the distance between the electrodes. Results indicated an increase in overpotential with increased electrode separation distance. This behavior was attributed to an increased resistance to electrolyte charge balancing by the electrolyte counter-ion, K^+.

Based on the results of the electrode separation distance study, it was hypothesized that adding a material with ionic activity between the electrodes would aid in electrolyte charge balancing and would result in reduction of overpotentials associated with electrode separation. The first PBEFB configuration was used in these studies. Initial results indicated that using an anion exchange resin, Amberlyst A-26(OH), exhibited lower overpotentials when compared against using a non-ionically active material, stainless steel shot, as the separation material. A survey of materials with different ionic activities was conducted based on these initial results. The survey of materials included: Amberlyst A-26(OH) basic ion exchange resin, Amberlite IR-120H acidic ion exchange resin, stainless steel shot, ethylene-acrylic acid copolymer beads, and ALL-CRAFT 4K activated carbon. The results indicated that Amberlyst A-26(OH) outperformed Amberlite IR-120H, but the ALL-CRAFT 4K activated carbon outperformed both of these materials. The copolymer beads and stainless steel shot performed about the same and exhibited the worst performance of materials tested. Particle size was ruled out as a possible reason for why ALL-CRAFT 4K outperformed Amberlyst A-26(OH) as a test with the use of similar particle sizes did not reveal similar results.

The effect of electrode separation distance while using ionically active separation materials was studied using the second PBEFB configuration. Amberlyst A-26(OH) and stainless steel shot were chosen as separation materials for these studies. Separation material beds of 2.2-, 2.8-, 4.1-, and 5.4-cm were used to separate the electrodes. The use of Amberlyst A-26(OH) as the separation material resulted in a 56% reduction in the voltage range (after 30 minutes of discharge) between 2.2- to 5.4-cm of electrode separation compared to the use of stainless steel shot. An important result of this study is that operating the PBEFB at 5.4-cm of electrode separation using Amberlyst A-26(OH) as the separation material exhibited better performance than using stainless steel shot as the separation material at only 2.2-cm of electrode separation.

The second PBEFB configuration was used to investigate the impact of electrolyte flow direction. It was hypothesize that electrolyte flow direction would have an impact on PBEFB performance due to possible differences in the mechanisms needed to maintain electrolyte charge balance. Using Amberlyst A-26(OH) and Amberlite IR-120H as electrode separation materials, the results were inconclusive. Neither flow direction with either separation material appeared to significantly affect PBEFB performance.

The research presented in this dissertation validates the use of packed-bed electrodes in a flow battery architecture and indicate that adequate electrode separation can be used by implementing ionically active electrode separation materials to reduce overpotentials. Adequate electrode separation is desired with the use of high

energy dense metallic negative active materials. The vertically stacked electrode PBEFB configuration exhibits significant promise as an improve flow battery design.

CHAPTER 1. INTRODUCTION

Electrochemistry is a branch of chemistry that is concerned with the relationships between chemical reactions and electricity.[1] Complete chemical reactions can be separated into half reactions, and in doing so, make it possible to isolate the electrons for use in various devices that require electrical power. The half reaction that produces the electrons is called an oxidation reaction, while that half reaction that consumes the electrons is called a reduction reaction. Example oxidation and reduction reactions are shown below in Equations 1.1 and 1.2, respectively.

$$Zn + 2OH^- \ <=> \ ZnO + H_2O + 2e^- \quad (1.1)$$

$$2MnO_2 + 2e^- + H_2O \ <=> \ Mn_2O_3 + 2OH^- \quad (1.2)$$

Electrochemical energy storage devices, such as batteries, are designed to physically separate these oxidation and reduction reactions at separate electrodes. The electrode where the oxidation reaction occurs is known as the anode and the electrode where the reduction reaction occurs is known as the cathode.

In conventional battery designs the anode and cathode are separated by a very thin sheet of material called a separator.[2] This separator prevents direct physical contact between the active materials of the anode and the cathode to prevent electrons from being shared. If the anode and the cathode were in direct contact, the electrons could not be completely isolated for use by an external device. An external path such as

a wire or a circuit of an electronic device facilitates the electron transfer from the anode to the cathode. Apart from an anode, a cathode, and an external electron path, an electrochemical energy storage device must also have a means to facilitate ion transfer between the anode and cathode.[2] For example, in the reduction reaction of Equation 1.2, 2 hydroxide ions (OH^-) are generated and they must be removed from the reaction site as not to hinder further reaction. It also shown in the oxidation reaction of Equation 1.1 that 2 hydroxide ions are needed for the reaction to proceed, thus the hydroxide ions generated at the cathode must diffuse across the inter-electrode space to the anode for the reactions to continue.

In typical batteries ion migration is accomplished through the use of a concentrated solution containing the ion requiring inter-electrode transfer. In the case of an electrochemical energy storage device using the reactions in Equation 1.1 and 1.2, a concentrated solution of sodium hydroxide (NaOH) or potassium hydroxide (KOH) in deionized water would provide the required hydroxide ions needed for the ion "bridging" across the inter-electrode space. In Figure 1.1, an illustration of the electron and ion transfer routes required for proper operation of an electrochemical energy storage device is shown through a schematic of a basic laboratory battery assembled in a beaker.

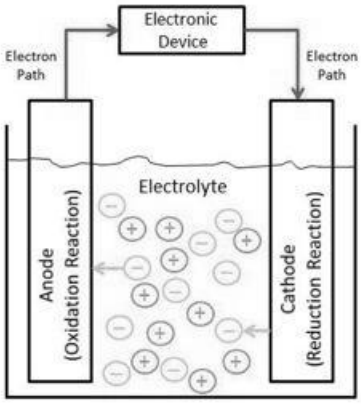

Figure 1.1. Schematic of a basic battery illustrating electrode separation, electron flow through an external path, and proportionate negative ion path through an electrolyte solution.

All batteries are classified into 2 categories; primary and secondary. Primary batteries are single use batteries that cannot be recharged very easily or reliably. The materials used in the production of primary batteries are what make them unable to be recharged effectively. Upon recharging, primary battery anode materials do not retain their original shape, and this can eventually lead to short-circuit risks.[3]

Apart from the primary/secondary classification, there are 2 types of battery designs. The batteries used by millions of people around the world to power their cell phones and laptop computers are diffusion-based designs. In a diffusion-based design, the ion migration from electrode to electrode is driven by ion concentration and voltage gradients between electrodes and the electrode separation must be minimized to optimize performance. The second battery design uses flowing electrolyte to deliver reactive ions between the electrodes. Because of the pumping required for electrolyte

circulation, these batteries are only suited for applications where the pumping system can be tolerated. Ideal applications for flow batteries are point-of-source electrical energy storage for the power grid and as a power source for electric vehicles (with further improvement).

The research presented in this dissertation is focused around a novel packed-bed electrode flow battery architecture.[4] A packed-bed electrode is a column of closely contacted granular battery materials that contains void space around the granules to allow for electrolyte flow through the packed-bed electrode. A flowing electrolyte is used to deliver reactive ions in solution at rates faster than could be achieved by diffusion alone. The combination of the three dimensional packed-bed electrodes and flowing electrolyte provide many benefits over other flow battery and conventional battery designs and these will be a topic of discussion in upcoming chapters of this dissertation.

The research presented in this dissertation provides insight into effects of the packed-bed electrode separation, provides strategies to obtain better performance at increasing electrode separation distances, and compares performance using a stationary versus flowing electrolyte in this new flow battery architecture. The packed-bed electrode flow battery is believed to be the next logical step in flow battery advancement, as the unique electrode structure provides opportunities to improve upon the specific energy (Wh kg^{-1}) of existing flow batteries.

CHAPTER 2. CURRENT ELECTRIC VEHICLE BATTERY TECHNOLOGY

2.1 Background of Electric Vehicle Technology

Prior to Henry Ford's invention of the mass-production process of gasoline fueled automobiles, early electric vehicle technology was cost effective for consumers. Thomas Edison developed a very robust Fe/NiOOH battery designed for electric vehicle use and it was first marketed in 1904. The beginning of the mass production of gasoline automobiles in 1910 made that technology more affordable than electric vehicles of the time and the idea of the electric vehicle soon diminished.[5]

It wasn't until the oil embargo of 1973 that, again, electric vehicles and their battery technology became an economically viable transportation option. The situation changed once the oil embargo came to an end. At the end of the oil embargo, gasoline availability, and therefore price, improved and once again the notion of electric vehicle transportation was abandoned.[5]

Renewed interest in electric vehicles began in the 1990's due to environmental regulations and mandates by the state of California.[6] A product of this period was the development of General Motor's first production attempt at an electric vehicle, the EV1. The first generation EV1 utilized a lead-acid battery system, which provided a range of 80-100 miles. Second generation EV1's used a nickel-metal hydride battery system that provided a range of 100-140 miles. Due to a weak demand and no financial viability General Motors eventually abandoned EV1 production.[7] Late in the decade, the first

Toyota Prius went on sale first in Japan in December 1997 and became the first mass-produced hybrid-electric vehicle.[8] This first generation Prius utilized nickel-metal hydride cylindrical shaped cells assembled into battery modules.[9]

High and ever-fluctuating oil prices, consumer environmental awareness, and advances in lithium-ion battery technology have again stimulated interest in electric vehicle technologies in the 2000's. An increase in the performance and decrease in the cost have made lithium-ion batteries increasingly attractive for use in electric vehicle technologies. Despite the improvement of lithium-ion technology, Toyota continued to use nickel-metal hydride batteries in the Prius when it launched in the United States in July 2000.[8] In 2008, Tesla Motors took an all-electric lithium-ion powered high-performance sports car to market.[10]

2.2 Nickel-Metal Hydride Battery

2.2.1 Introduction

Nickel-metal hydride (NiMH) battery technology dates back to the 1960s, and it is still used in specific applications today. The NiMH battery was designed as an improved replacement of the nickel-cadmium (NiCd) battery that was used in portable electronics of the era. NiMH battery research led to dramatic improvements over the NiCd battery and the 30-50% increase in the energy density of the NiMH over the NiCd was the most important of these improvements. Also, the fact that the NiMH battery contained non-toxic and environmentally friendly components and that natural resources were abundant in these components made the NiMH battery a good

replacement for the NiCd battery. The NiMH battery was first made available to the public when it was commercialized in 1990.[11]

2.2.2 Electrochemistry of the Nickel-Metal Hydride Battery

NiMH battery cells have a voltage between 1.25 V and 1.35 V while sitting idle(not being charged or discharged), an operating voltage of 1.2 V, and once NIMH battery cells reach 1.0 V, they are at the end of their useful life. The positive electrode (cathode) active material of the NiMH battery in the charged state is nickel oxyhydroxide (NiOOH) and the negative electrode (anode) active material in the charged state is hydrogen contained in a metal hydride (MH). NiMH batteries use aqueous solutions of potassium hydroxide as electrolyte. The negative and positive electrode electrochemical half reactions of the NiMH battery are shown below in Equations 2.1 and 2.2, respectively.

$$MH + OH^- <=> M + H_2O + e^- \quad (2.1)$$

$$NiOOH + H_2O + e^- <=> Ni(OH)_2 + OH^- \quad (2.2)$$

Overcharging the NiMH battery can produce oxygen which can become a safety issue due to increasing the internal pressure of the battery. The use of a negative electrode with a higher effective capacity than the positive electrode causes the positive electrode to reach a fully charged state before the negative electrode. Once the positive electrode is completely charged, further charging begins to oxidize the

hydroxide ions at the positive electrode producing oxygen gas and water. This over-charge reaction is shown below in Equation 2.3.

$$2OH^- <=> H_2O + \frac{1}{2}O_2 + 2e^- \quad (2.3)$$

The generated oxygen gas diffuses across the membrane separator to the negative electrode where it participates in the following reaction.

$$4MH + O_2 <=> 4M + 2H_2O \quad (2.4)$$

The reaction in Equation 2.4 prevents the negative electrode from ever being completely recharged, but is effective at managing the oxygen gas generation to prevent cell pressurization. NiMH batteries are designed with an excess of negative electrode active material to allow this oxygen recombination reaction to proceed without adversely effecting battery operation.[12]

2.2.3 Drawbacks of the Nickel-Metal Hydride Battery

Despite the NiMH battery popularity for use in current hybrid electric vehicles, it has a few drawbacks. With heavier active materials and a dramatically lower operating potential, the NiMH battery contains only about one-half the specific energy (Wh kg^{-1}) of a lithium-ion battery.[5] The NiMH battery maximum capacity is moderately affected by repeated charging without complete discharges (memory effect) and has poor charge retention (shelf life).[12]

2.3 Lithium-Ion Battery

2.3.1 Introduction

Sony Inc. first commercialized the lithium-ion battery in 1991 and it quickly captured the personal electronics market.[13] The initial specific energy of the lithium-ion battery was around 100 Wh kg^{-1} in 1991 and persistent research activity improved that value to over 200 Wh kg^{-1} (about two times the specific energy of NiMH battery) by 2008.[14] Lithium-ion batteries typically use a carbon negative electrode (anode) material in which the lithium-ions can intercalate between the graphene sheets of the carbon material upon charging. Many types of positive electrode (cathode) materials can be used in lithium-ion batteries and each cathode material changes the operating parameters of that battery. Commercially available lithium-ion batteries typically use lithium cobalt oxide, $LiCoO_2$, as the cathode active material[15], but the newest commercially available lithium-ion battery uses lithium-iron phosphate, $LiFePO_4$, cathode material. Lithium-iron phosphate initially suffered from poor electrical conductivity, but recent improvements, such as using smaller sized particles[16] and doping techniques[17], have improved the electrical conductivity of the material. A lithium-iron phosphate lithium-ion battery can be discharge very quickly, which means it can also be charged very quickly.[5] Lithium-iron phosphate is inherently safer than other cathode materials due to more thermal stability.[18]

In 2008, Tesla Motors released a high performance, all-electric sports car that uses lithium-ion batteries.[19] This was the first electric automobile to take advantage of a lithium-ion battery pack. Toyota had been testing lithium-ion battery packs in their

Prius hybrid-electric vehicle (HEV), but at the conclusion of their testing they decided to continue to use NiMH battery packs in their hybrid Prius.[20] Toyota is planning to implement lithium-ion battery packs in their upcoming plug-in hybrid-electric (PHEV) Prius.[21]

2.3.2 Electrochemistry of the Lithium-Ion Battery

Lithium-ion battery cells operate in a potential range of 2.5 V to 4.1 V depending on the positive and negative electrode active materials used. As discussed above many different positive electrode active materials are used and each has their own advantages/disadvantages. The choice of positive electrode material has a direct influence on the cell potential and specific capacity as the cell capacity is usually limited by the positive electrode. Table 2.1 compares the specific capacity, potential, and advantages/disadvantages of some different positive electrode materials used in lithium-ion battery cells.

Table 2.1. Comparison of lithium-ion cell positive electrode material characteristics.[22]

Material	Specific Capacity (mAh/g)	Midpoint V vs. Li (@ 0.05C)	Advantages/Disadvantages
$LiCoO_2$	155	3.88	Most common, Co is expensive
$LiNi_{0.7}Co_{0.3}O_2$	190	3.70	Intermediate cost
$LiNi_{0.8}Co_{0.2}O_2$	205	3.73	Intermediate cost
$LiNi_{0.9}Co_{0.1}O_2$	220	3.76	Highest specific capacity
$LiNiO_2$	200	3.55	Most exothermic decomposition
$LiMn_2O_4$	120	4.00	Mn is less expensive, low toxicity, least exothermic decomposition

Graphite or a mixture of carbons is typically used as the negative electrode in lithium-ion batteries. The carbons allow the lithium ions to be inserted between the structure of their graphene sheets upon charging.

Lithium-ion batteries use organic solvents as the basis for their electrolyte systems. Similar to the selection of positive electrode materials, there are a number of different electrolyte compositions that can be used. They are typically composed of a mixture of 2 or more organic solvents with 1 or 2 different lithium containing solutes[22], and sometimes include additives to improve extreme temperature performance[23] or fire retardency[24]. The constant pursuit of an improved lithium-ion battery electrolyte makes it a popular research focal point.

Most commercial lithium-ion batteries are composed of cells using a carbon host negative active material and a lithium cobalt oxide positive active material. These active materials exist in thin layers on current collectors and are separated by a thin, electrical insulating, and ion conducting separator. The half reactions occurring at the negative and positive electrodes are shown below in Equations 2.5 and 2.6, respectively.

$$Li_xC \ <=> C + xLi^+ + xe^- \tag{2.5}$$

$$Li_{1-x}CoO_2 + xLi^+ + xe^- \ <=> LiCoO_2 \tag{2.6}$$

It is important to note that in this technology no lithium metal is formed at the positive or negative electrode. The lithium-ions are held in ion form between the metal oxide layers at the positive electrode and between the graphene layers at the negative

electrode. The absence of lithium metal makes lithium-ion batteries safer, less reactive, and offer longer cycle life when compared to lithium metal batteries. Over-charging or –discharging can cause significant problems in the cell and these are prevented using protection circuitry in the battery pack.[22]

2.3.3 Drawbacks of the Lithium-Ion Battery

Lithium-ion battery technology controls most of the personal electronics market, but currently has only made a small entry into the automotive market. There are a few major challenges that must be overcome before lithium-ion batteries can be applied on a large scale to vehicle technology; these are safety and cost.

Safety is perhaps the number one challenge for battery engineers. The overcharging of lithium-ion batteries can lead to internal short-circuits, which in turn leads to a violent reaction that can cause the battery to catch fire.[25] To combat this problem, protection circuitry must be employed at the cell and battery pack level to prevent over charging.[5] Overheating of lithium-ion batteries can also lead to battery failure ultimately resulting in fire.[25]

The cost of lithium-ion batteries is the second major challenge inhibiting their use in electric vehicles. Lithium-ion batteries were initially (circa 1991) very expensive at about \$20,000 kWh^{-1} and therefore could only be applied to situations where costs could be tolerated.[5] At that price, the 53 kWh battery pack of today's Tesla Roadster[26] would cost about \$1 million, which would be totally unacceptable to consumers. Continued research focused on reducing the cost of lithium-ion batteries brought their

costs down to \$400-\$750 kWh^{-1} by the year 2000.[27] Even at \$750 kWh^{-1}, the 53 kWh battery pack would still cost about \$40,000. This is still an unacceptable cost if the automobile industry is trying to build an affordable electric vehicle that sells for less than \$30,000. PHEVs can be made more affordable by using a much smaller battery pack, limiting their all-electric driving range, because they have the benefit of a gasoline generator to provide power once the all-electric driving range is surpassed. Based on a United States Advanced Battery Consortium estimated 11.6 kWh battery pack size for a PHEV with 40 miles of all electric range (PHEV-40)[28], the PHEV-40 battery pack would cost about \$9,000 (at \$750 kWh^{-1}). \$9,000 for a battery pack might be feasible if the battery pack can last the life of the vehicle, but if consumers have to replace this battery sometime during the life of the vehicle then the initial purchase doesn't seem feasible any longer.

2.4 Conclusion

NiMH batteries are currently the battery of choice for electric vehicle applications based on their proven history. Unfortunately, NiMH batteries have a very low specific energy, and therefore NiMH battery packs for electric vehicle use are very heavy. The higher specific energy of lithium-ion batteries over NiMH batteries make them more attractive for electric vehicle applications, but their safety concerns and high costs have been prohibitive. Research over the last 20 years has dramatically reduced safety issues and costs, but continued research efforts focused on these issues are still needed before lithium-ion batteries can capture the entire electric vehicle market.

CHAPTER 3. REVIEW OF FLOW BATTERY TECHNOLOGY

3.1 Redox Flow Battery

3.1.1 Introduction

Redox flow batteries (RFBs) were first conceptualized by Thaller at NASA as a bulk electrical storage device.[29] RFBs use soluble active materials in 2 half-cells separated by an ion-selective membrane and inert electrodes provide surface area for electron transfer reactions to occur. Figure 3.1 is a schematic of a RFB. Thaller theorized that RFBs would benefit from high overall efficiency, no cycle life limitations of electrodes, and deep discharge capability. While Thaller predicted relatively low specific energies of RFBs, he stated that applications requiring high efficiencies would benefit from the application of RFBs.[29]

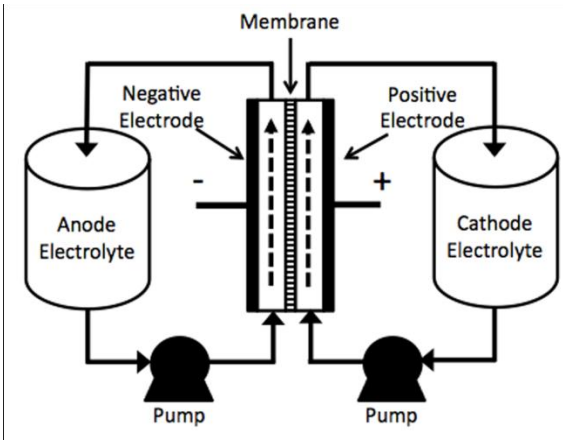

Figure 3.1. Schematic of a redox flow battery.

There are a few major advantages of the RFB design. The unique design of RFBs allow the separation of energy storage capacity from the available power. The energy storage capacity is determined by the concentration and volume of electrolytes, while the power is determined by the surface area of the electrodes and the number of redox flow cells assembled into the stack of the RFB. With all active materials present in the electrolytes of each half-cell, RFBs have the distinct ability to be recharged by replacing the electrolytes in a discharged state with fresh electrolytes in a recharged state.[30] Chemical recharging allows the RFB to be fully recharged quicker than if it were electrically recharged.

3.1.2 Redox Flow Battery Technologies

3.1.2.1 Iron-Chromium Redox Flow Battery

The iron-chromium (Fe/Cr) redox flow battery (RFB) was one of the first RFBs developed. In 1979, the Fe/Cr RFB was developed by NASA to provide electrical energy storage for remote power systems that use solar or wind energy resources. The iron-chromium RFB was sought as a reduced maintenance and cost effective replacement for conventional design lead-acid batteries that were currently being used with remote power systems.[31] The chemistry of the Fe/Cr RFB involves the redox couples Fe^{+2}/Fe^{+3} (positive electrode) and Cr^{+2}/Cr^{+3} (negative electrode) that are supplied by 1 molar solutions[32] of $FeCl_2$ and $CrCl_3$ in 2 normal HCl solutions[33]. The negative and positive electrode reactions are shown below in Equations 3.1 and 3.2, respectively, with

discharge reactions orientated from left to right and charge reactions orientated from right to left.

$$Cr^{+2} <=> Cr^{+3} + e^{-} \quad (3.1)$$

$$Fe^{+3} + e^{-} <=> Fe^{+2} \quad (3.2)$$

Membranes separating the positive half-cell from the negative half-cell must be highly prohibitive to transfer of iron and chromium through the membrane. Transfer of these ions across the membrane results in the reduction in the current efficiency of the RFB, as the ability to produce current is lost for any materials crossing into the opposite half-cell. The membrane separator must allow for the transfer of non-reacting ions such as H^+ and Cl^- as they must transfer from half-cell to half-cell as current is passed between the half-cells to maintain charge balance inside the RFB.[32] Both anionic[34] and cationic[35] membranes have been used as separators in the Fe/Cr RFB, with each providing varied performance due to their respective transfer properties.

There are a few major issues with the Fe/Cr RFB. First, the reduction reaction of Cr^{+3} to Cr^{+2} is a relatively slow reaction[36] and it is too slow a reaction rate for battery use without the aid of a catalyst. Another major issue is that hydrogen is evolved from the negative half-cell electrolyte before Cr^{+3} can be reduced. Hydrogen evolution reduces current efficiency of the cell, and if hydrogen evolution continues, it can lead to an imbalance between the electrolytes of the 2 half-cells. This imbalance results in an irreversible loss of cell capacity.[37] Initially a 2-step catalysis process was developed to handle the poor Cr^{+3} reduction kinetics and the hydrogen evolution problem in the

negative electrode half-cell. A small amount of gold was plated into the inert electrode and then a small amount of lead was plated onto the gold. Upon charging, the electrode then acts as a lead electrode and works to prevent hydrogen evolution.[38] Investigations into using bismuth and bismuth-lead catalysts have also proved to be effective at increasing the reversibility of the chromium reaction and reduction of hydrogen evolution rates.[39] Small imbalances due to hydrogen evolution or the air oxidation of the chromium or iron species are corrected by a rebalance cell. The rebalance cell keeps the positive and negative half-cell electrolytes at the same state of charge by employing a hydrogen electrode.[37] Another drawback of the Fe/Cr RFB is that it exhibits a relatively low specific energy of around 15 Wh kg^{-1}, which is about half of that of the lead-acid battery.[30] The low specific energy is irrelevant for land-based energy storage systems such as those for remote power systems, but is prohibitive for use in mobile applications.

3.1.2.2 All-Vanadium Redox Flow Battery

In response to the shortcomings of the Fe/Cr RFB, the all-vanadium RFB (AVRFB) was developed in 1986.[40] The AVRFB operates using V^{+3}/V^{+2} redox couple on the negative electrode side and V^{+5}/V^{+4} couple on the positive electrode side.[30] The negative and positive half-cell electrochemical reactions are shown below in Equations 3.3 and 3.4, respectively. Initially, 0.1 molar solutions of V(III) and V(IV) in 2 molar sulfuric acid (H_2SO_4) solutions were used as the electrolyte solutions in the negative and positive electrode half-cells, respectively.[40] After an investigation of different vanadium

compounds in several different solvents, vanadyl sulfate ($VOSO_4$) in sulfuric acid (H_2SO_4) solution was later chosen as the electrolyte solution for both half-cells of an AVRFB.[30]

$$V^{+2} <=> V^{+3} + e^{-} \quad (3.3)$$

$$V^{+5} + e^{-} <=> V^{+4} \quad (3.4)$$

In the AVRFB, the separation membrane is single most source of performance loss. Undesired water transfer through the separation membrane from one half-cell to the other half-cell can eventually have negative effects on the AVRFB performance. Water transfer across the membrane causes one half-cell electrolyte to become diluted, while the other half-cell electrolyte becomes concentrated. This concentration imbalance causes a loss of cell performance, as the active material concentrations are directly related to cell voltage. Water can be transferred across the membrane by ions moving due to concentration gradients, carried by charge balancing ions, or due to pressure differences between the half-cells. Although the separation membranes are usually sufficiently resistant to water transfer, the rate of water transfer increases with increased exposure to vanadium electrolyte solutions.[41]

Modifications have been made to membranes to decrease the amount of water transfer in an AVRFB. Mohammadi and colleagues modified a Selemion AMV anion exchange membrane by sulfonation to produce strong cation exchange groups in the membrane's structure and this proved beneficial in reducing the amount of water transferred through the membrane.[42] Sukkar and colleagues modified a cation exchange membrane by soaking the membrane in anionic and cationic polyelectrolyte

solutions. It was believed the cationic polyelectrolytes would reduce the ion exchange capabilities of the membrane by binding with the anionic co-ions present in the cationic exchange membrane. The anionic polyelectrolytes were suspected to enter the pores of the cationic exchange membrane where they would precipitate and partially block the pores preventing water transfer through the membrane. Initial improvement in water transfer properties was confirmed, but after prolonged exposure to vanadium solutions the improved properties diminished.[41] A third attempt to improve water transfer properties of the AVRFB separation membrane was pursued by Zeng and colleagues and consisted of electrolyte soaking, oxidation polymerization, and electrodeposition techniques using pyrrole to modify Nafion117 proton exchange membranes. While it was found that all three of these techniques improved water transfer properties of the Nafion membrane, the electrodeposition technique proved to be the most beneficial by reducing the water transfer rate to a third of its original value.[43]

Large separation membrane resistivity has negative effects on the AVRFB performance. Membrane resistivity is discussed in terms of the selectivity of H^+ transfer through the membrane. It is important to allow H^+ to transfer through the membrane between both half-cells so that charges can be continually balanced as electric current is passed from the half-cell to half-cell. The hindrance of H^+ transfer through the membrane provides for a higher membrane resistivity and leads to a reduction in supplied voltage, thus a decrease in voltage efficiency.[44] Efforts to synthesize membranes with decreased resistivity resulted in great success. Chen and colleagues developed a sulfonated polymer membrane with vastly improved proton transfer

properties compared to Nafion117. Nafion is often used as a benchmark material because of its excellent proton transfer and chemical resistance.[45] In another case, cation exchange groups were added to a polysulfone (Psf)-polyphenylenesulfidesulfone (PPSS) copolymer by polymerizing it with tungstophosphoric acid. This synthesized cation exchange membrane exhibited smaller differences in cell resistivity between charging and discharging at both 0% and 100% states of charge when compared with Nafion117, indicating more consistent proton transfer across the entire operating range of the AVRFB.[44]

The development of the AVRFB has proved to offer key improvements over the Fe/Cr RFB. The elimination of the need for catalyst and a rebalance cell lead to reduced design and production costs of a RFB. The use of a single metal active material in both half-cells has eliminated permanent performance loss upon cross-contamination. In the AVRFB, the cross-contamination of vanadium-ions of different oxidation states lowers the current density for that cycle and the vanadium-ions in each half-cell can be returned to their correct oxidation states by simply recharging the AVRFB.[46] Despite the inherent improvements of the AVRFB over the Fe/Cr RFB, membrane modification and synthesis are continually looking to improve the performance of the AVRFB. With a specific energy of about 25 Wh kg-1 the AVRFB has almost double the specific energy of the Fe/Cr RFB and was competitive with leading conventional battery technologies of the time, nickel/cadmium and lead/acid.[30] This increase in specific energy from the Fr/Cr RFB to the AVRFB initiated the idea that these RFB technologies may eventually be applicable to mobile applications.

3.1.2.3. Vanadium Chloride/Polyhalide Redox Flow Battery

A vanadium chloride/polyhalide RFB was investigated by Skyllas-Kazacos in an effort to increase the specific energy of a vanadium-based RFB. The AVRFB is limited to a 2 molar vanadium ion concentration[47] (2M $VOSO_4$ in H_2SO_4) and this limits the specific energy of the system. Increased concentrations, up to 4M, of V(II) and V(III) can be achieved in the negative half-cell by using VCl_2 and VCl_3 dissolved in hydrochloric acid (HCl). Unfortunately, the HCl cannot be applied to the positive half-cell of an AVRFB because the chlorine ions in the HCl solution reduce the V(V) to V(IV) while producing potentially hazardous chlorine gas.[48] In order to take advantage of the higher solubility of the hydrochloric acid based electrolyte, a new positive half-cell redox couple was sought that would remain stable in such solutions. The polyhalide ion $ClBr_2^-$ (or $BrCl_2^-$) was selected as the positive half-cell active material as it has chlorine in common with the negative half-cell, and that it was expected to behave similar to Br_3^-, which has been used in a positive half-cell redox couple in the sulfur-bromine RFB.[47] The negative and positive half-cell reactions for the vanadium chloride/polyhalide RFB are shown below in Equations 3.5 and 3.6(a or b), respectively, with discharge reactions occurring from left-to-right and charge reactions occurring from right-to-left.

$$VCl_2 + Cl^- <=> VCl_3 + e^- \quad (3.5)$$

$$BrCl_2^- + 2e^- <=> Br^- + 2Cl^- \quad (3.6a)$$

$$ClBr_2^- + 2e^- <=> 2Br^- + Cl^- \quad (3.6b)$$

3.1.2.4. Vanadium Bromide Redox Flow Battery

A vanadium bromide RFB was developed by Skyllas-Kazacos and colleagues at the University of New South Wales. This RFB uses the same redox couples as their vanadium chloride/polyhalide RFB discussed above (V^{+2}/V^{+3} and $ClBr_2^-/Br^-$), but takes advantage of vanadium bromide compounds instead of vanadium chloride compounds. The electrolyte solutions use both hydrochloric and hydrobromic acids as solvents and vanadium bromide as the ionic species.[49]

Vanadium bromide has a higher solubility than the vanadyl sulfate used in the AVRFB, and this has many benefits for the vanadium bromide RFB. The higher solubility of vanadium bromide provides almost double the specific energy (~50 Wh kg^{-1}) as compared to the AVRFB. Improved low temperature performance is directly related to increased solubility of the vanadium bromide. By using the additionally available bromine ions in the positive half-cell during charging, the positive half-cell electrolyte tank volume can be decreased by almost 50%, which there reduces the amount of total electrolyte of the system by 25%. This has a positive impact on the specific energy of the vanadium bromide RFB.[49]

A drawback of the vanadium bromide RFB was that there was the possibility of potentially hazardous bromine gas (Br^2) evolution upon charging. The use of bromine complexing agents was investigated to prevent this bromine gas evolution. Bromine complexing agents, such as polyethylene glycol and tetrabutylammonium bromide, work to prevent bromine gas evolution by binding with the bromine before it can

produce bromine gas molecules.[49] The loss of bromine by gas evolution would ultimately have a negative impact on the current efficiency of the vanadium bromide RFB.

3.1.3 Summary

Although not every redox flow battery system was discussed in the preceding discussion, the monumental first redox system and the heavily researched vanadium based redox flow battery systems were presented. Since the initial concept of a redox flow battery, there have been great strides in the development of redox flow batteries. Within the first 7 years, the evolution from the iron-chromium redox flow battery to the all-vanadium redox flow battery provided a 40% increase in the specific energy. This success is attributed to improved reactions with more favorable kinetics and reversibility, improved higher concentration electrolyte systems, and improved membrane performance due to chemical modification and synthesis. Current redox flow battery specific energies are sufficient for stationary energy storage applications, but they must be increased for redox flow batteries to eventually be applied to automobile applications.

3.2 Hybrid Flow Battery

3.2.1 Introduction

Hybrid flow batteries (HFBs) offer some key advantages over the conventional redox flow batteries discussed above. As seen in Figure 3.2, the HFB uses only a single flowing electrolyte, so there is no need for a separation membrane to separate the

electrodes into half-cells. The elimination of the separation material offers significant material cost savings and also eliminates all of the potential issues associated with using separation membranes, such as water transfer, cross-contamination, and membrane resistivity. The use of a single flowing electrolyte eliminates the capital cost associated with a second pumping system and reduces the operating cost of pumping.

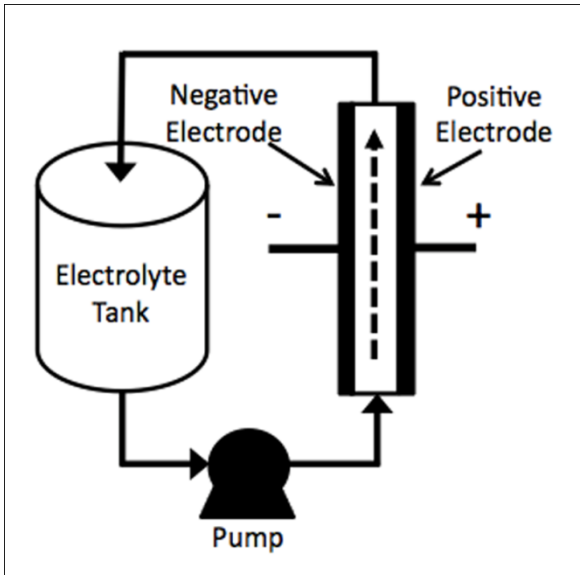

Figure 3.2. Schematic of a hybrid flow battery.

The term "hybrid" is used because HFBs typically use a positive electrode that involves a solid-phase to solid-phase electrochemical reaction and the negative active material exists as a soluble species in the electrolyte while in the discharged state, but as an electrodeposited solid in the charged state. Therefore, the use of both solid-phase and soluble active materials makes the HFB a hybrid of the redox flow battery and conventional diffusion-based battery. Because solid phases are involved, drawbacks to these hybrid systems typically involve positive electrode solid phase transitions that

render the material less electrochemically active or less efficient and problems with material deposition/dissolution at the negative electrode.

3.2.2 Hybrid Flow Battery Technologies

3.2.2.1 Soluble Lead(II) Flow Battery

In 2004, a novel lead-based flow battery was developed. The soluble lead(II) flow battery (SLFB) eliminated the need for separating the positive and negative electrodes into half-cells by only requiring a single flowing electrolyte to supply Pb^{+2} ions to both electrodes.[50] The SLFB uses a 1.5 molar lead methanesulfonate in 0.9 molar methanesulfonic acid electrolyte solution. The electrolyte concentration was selected so that Pb^{+2} would be soluble at all states of charge.[51] The negative and positive electrode reactions of the SLFB are shown below in Equations 3.7 and 3.8, respectively, with discharge reactions oriented from left to right and charge reactions oriented from right to left. By eliminating the need for separated half-cells, the need for expensive, specialized separation membranes was eliminated. The use of a single flowing electrolyte reduced overall system weight, capital cost, and operating cost compared to redox flow batteries that require 2 flowing electrolytes.

$$Pb \;<=>\; Pb^{+2} + 2e^- \tag{3.7}$$

$$PbO_2 + 4H^+ + 2e^- \;<=>\; Pb^{+2} + 2H_2O \tag{3.8}$$

In addition to not requiring a separator and only using a single flowing electrolyte, the SLFB has another great benefit of being able to continually endure deep

discharges while maintaining cycle life. The SLFB is unique in that both positive and negative reactions involve the electrodeposition/dissolution of active materials to/from inert electrodes. The lack of solid-phase to solid-phase transitions upon cycling eliminates volume expansion issues that can lead to irreversible electrode damage during deep discharge. This allows the SLFB to be deeply discharged without sacrificing cycle life.[52] Volume expansion damage plagues the conventional lead-acid battery and prevents its use in deep discharge applications.

In order for the SLFB to maintain a long cycle life, the electrodes must return to their original state after each full cycle. It was proposed that the electrodes could only return to their original states if each exhibited the same current efficiencies their respective reactions. As it turns out, there is a difference in the current efficiencies between the positive and negative electrodes, and a slight amount of Pb is left on the negative electrode after each cycle. For this reason, the SLFB must be rebalanced on occasion to remove the accumulation of Pb on the negative electrode. The rebalancing is completed by draining the electrolyte from the SLFB and flowing oxygenated methanesulfonic acid through the battery without exchanging current between the electrodes. The reaction for this rebalancing process is shown below in Equation 3.9.[51]

$$2Pb + 4H^+ + O_2 \Rightarrow 2Pb^{+2} + 2H_2O \qquad (3.9)$$

3.2.2.2 Zinc-Nickel Flow Battery

The zinc-nickel flow battery (ZNFB) uses a single flowing electrolyte composed of 1 molar ZnO in 10 molar KOH and does not require a separation membrane. The

negative and positive electrode reactions for the ZNFB are shown below in Equations 3.10 and 3.11, respectively, with discharge reactions oriented from left to right and charge reactions oriented from right to left. At the positive electrode of the ZNFB a solid-phase to solid-phase transition occurs between NiOOH and $Ni(OH)_2$ as the battery is cycled. At the negative electrode, the $Zn(OH)_4^{-2}$ ions are reduced to Zn metal at the electrode surface during charging. The reverse process occurs upon discharging.[53]

$$Zn + 4OH^- \ <=> \ Zn(OH)_4^{-2} + 2e^- \qquad (3.10)$$

$$2NiOOH + 2H_2O + 2e^- \ <=> \ 2Ni(OH)_2 + 2OH^- \qquad (3.11)$$

A preliminary study of the ZNFB used nickel foil as the inert negative substrate material while nickel(II) hydroxide was used as the positive electrode active material. The results of study revealed that a large overpotential was associated with the negative electrode (voltage loss) and that residual zinc remained on the negative substrate at the end of discharging, which leads to uneven deposition when zinc is re-deposited. A loss of positive electrode active material was seen with increased cycling. The loss of positive active material leads to capacity loss of the positive electrode. Electrode material loss is typical in situations where solid-phase to solid-phase transitions occur during cycling.[53]

In conventional batteries, the electrode substrate does not play a large role in the cell performance, but complete active material dissolution into the electrolyte reveals a bare substrate that then has a direct impact on flow cell performance. In response to the overpotential and electrodeposition/dissolution issues in the

preliminary ZNFB study, an investigation of various negative electrode substrates was conducted. Copper, lead, and cadmium were investigated as substrate materials for use in the ZNFB. It was determined that a cadmium substrate provided for less hydrogen evolution, which provided for more efficient deposition of zinc. Using the cadmium substrate it was determined that there are large differences in the zinc deposit morphology between stationary electrolytes and flow electrolytes. The flowing electrolyte significantly prevented zinc dendrite formation, even at increasing current density.[54]

Zinc electrodeposition/dissolution would be considered to continue forever without problems as long as the zinc electrodeposited by the reduction process is completely dissolved into the electrolyte during the oxidation process for each cycle. For understanding the stability of the ZNFB, it would then be important to understand the stability of the positive nickel oxide electrode.[55] It has been shown that the inclusion of zinc in nickel hydroxides prevents the α- and β-phase transition to γ-phase nickel hydroxide. This phase transition is accompanied by a reduction in battery voltage.[56]

Positive electrode stability studies were conducted using electrolyte solutions with and without the presence of ZnO. In the absence of ZnO in the electrolyte, oxygen gas evolution and physical deformation was observed at the positive electrode after 400 charge/discharge cycles. Vast improvements were witnessed with the presence of ZnO in the electrolyte. The presence of ZnO drastically reduced oxygen gas evolution and

prevented the transformation of β-nickel hydroxides to γ-nickel hydroxides, thus preserving battery voltage. Although x-ray photoelectron spectroscopy (XPS) revealed the presence of zinc in the positive electrode, x-ray diffraction (XRD) did not indicate the presence of pure Zn or ZnO. This suggests that zinc may be intercalated into the structure of the nickel oxide electrode. The XRD analysis did indicate that there were no structural changes to the nickel oxide electrode after 400 cycles in the presence of electrolyte containing ZnO.[55]

3.2.2.3 Copper-Lead Dioxide Flow Battery

The copper-lead dioxide flow battery (CLDFB) was investigated based on properties of previous flow batteries and the lead-acid battery. The positive electrode involves a solid-phase to solid-phase transition between PbO_2 and PbSO4, while the negative electrode involves the electrodeposition/dissolution of copper on a graphite electrode. The CLDFB uses a 1 molar $CuSO_4$ in 1.9 molar H_2SO_4 electrolyte solution to provide copper and sulfate ions to the electrodes. The negative and positive electrode reactions are shown in Equations 3.12 and 3.13, respectively, with discharge reactions oriented from left to right and charge reaction oriented from right to left.[57]

$$Cu \ <=> \ Cu^{+2} + 2e^- \tag{3.12}$$

$$PbO_2 + 4H^+ + SO_4^- + 2e^- \ <=> \ PbSO_4 + 2H_2O \tag{3.13}$$

During the investigation, a surplus of PbO_2 is used in the positive electrode to keep the extent of reaction of the PbO_2 to around 50%. This provides for optimal current efficiency and prevents damage associated with deeply discharging the positive

electrode.[57] This is similar to the method employed in conventional lead-acid batteries, as deep discharging leads to a large volume change of the electrode material. Repeated electrode material volume changes can lead to the shedding of active materials, resulting in irreversible loss of capacity. Despite the effort to prevent the loss of PbO_2 at the positive electrode, PbO_2 powder was lost into the electrolyte and therefore some capacity was lost. Copper powder was also found in the electrolyte, so the negative electrode lost some capacity as well.[57] These powder losses were most likely related to poor adhesion to the electrode substrate material, as opposed to volume expansion issues.

3.2.3 Summary

Great efforts have been made improve upon the initial successes of redox flow batteries. The fundamental work on the soluble lead(II) flow battery has inspired others to pursue single flow, "hybrid" style flow batteries by combining principles from redox flow batteries and conventional diffusion-based batteries. The elimination of separate half-cells and the separation membrane make for less complicated systems. The use of a single flowing electrolyte saves on cost and improves specific energies with the elimination of a second pumping system. While there are many different chemistries being pursued as hybrid flow batteries, not one is perfect and further research is needed to improve the technology.

CHAPTER 4. NOVEL PACKED-BED ELECTRODE FLOW BATTERY

4.1 Introduction

Increasing flow battery specific energy is required for their application to electric vehicles. To increase flow battery specific energy, it is desired to use solid active materials that provide higher molar densities of active materials over soluble active materials. Recharging metallic negative materials can be problematic because uneven deposition can lead to dendrite formation.[58] It has been previously discovered that zinc dendrite formation can be drastically reduced by using electrolyte circulation.[54] Lower electrode current densities (mA cm^{-1}) also provide more uniform electrodeposition[59], so an increase in electrode surface area would also be beneficial in reducing dendrite formation. The use of a three-dimensional, flow-through, packed-bed electrodes could significantly increase electrode surface area without substantial increases in battery volume, as would be required with planar electrodes. A packed-bed electrode flow battery (PBEFB) is expected to provide the increased specific energy needed for electric vehicle applications by accommodating electrolyte flow and providing an increased electrode surface area per volume of material.

4.2 Description

The PBEFB is a novel approach to flow battery architecture. A PBEFB is configured very similar to a vertically-oriented packed-bed reactor used commonly by the chemical manufacturing industry for heterogeneous catalysis. A schematic of the PBEFB is shown below in Figure 4.1.

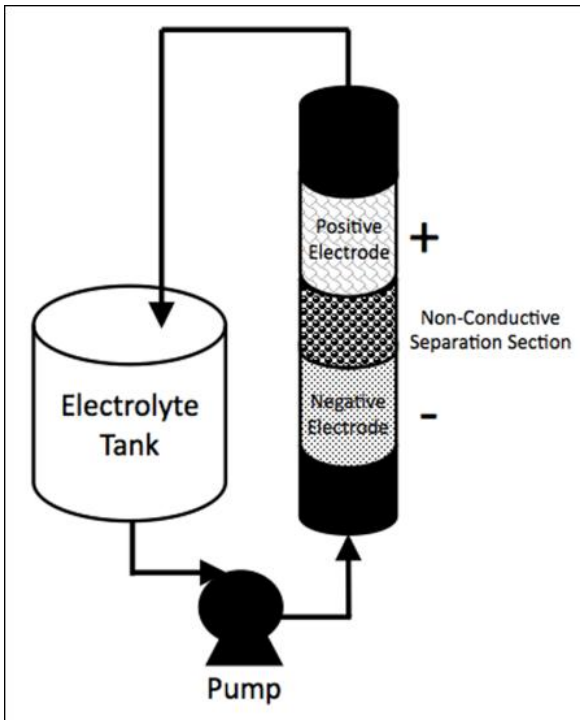

Figure 4.1. Schematic of packed-bed electrode flow battery.

The PBEFB has 2 electrode sections made of inert, conductive metal tubes to collect electrical current supplied by the packed-beds of granular active materials stored within. The electrode tubes are connected by a non-conductive coupling, in which non-conductive sheet material can be used to maintain electrode isolation. Other configurations will be discussed in upcoming chapters that allow for the use of granular separating materials. A single electrolyte solution is stored external to the PBEFB and is recirculated through the PBEFB using a single pump to supply reactive ions to the packed-bed electrodes.

4.3 Benefits

The PBEFB has numerous benefits over the conventional diffusion-based battery design. An increased surface area available for electrochemical reaction in less space is a benefit of using a three-dimensional packed-bed electrode over a standard planar electrode. In cases of extremely high electrical current discharge rates, the convective electrolyte flow of the PBEFB can deliver reactive ions to the electrodes faster than bulk diffusion alone. In these extremely high rate situations using convective electrolyte flow can provide thermal management for the PBEFB system by circulating it through a heat exchanger. This would be important to prevent thermal runway of the electrochemical reactions. The increased surface area of the packed-bed electrode helps to reduce local current densities (mA/cm^2) during high rate discharges from the PBEFB. This has a positive effect while trying to electrodeposit metallic active materials without the formation of dendrites. Since the electrical current is distributed over a large surface area in the packed-bed electrode, there is a more uniform current density and this provides for more uniform use of active materials throughout the packed-bed electrode. The reduction in electrode cross-sectional area from the conventional battery to the PBEFD leads to the reduction in the amount of separator material required. The separator materials can be highly specialized (thus quite expensive), so the reduction of the amount of separator provides an economic benefit. Similar benefits of the PBEFB are highlighted when comparing the PBEFB to typical flow battery architectures previously discussed.

Traditional chemical engineering principles provide an existing knowledge base for the design and scale-up of packed-bed systems and extending this knowledge base to PBEFB should be straight forward. For instance, this knowledge base reveals that increasing the available surface area of active materials in the packed-bed (reducing active material granule size) comes at the cost of increased pressure requirements to pump the electrolyte through the packed-beds.[60] This knowledge base can also provide insight into how electrolyte flow behavior through the packed-beds affects the mass transfer of reactive ions to the active material surfaces.[61] Taking advantage of this existing knowledge base should allow for a more timely advancement of packed-bed electrode flow battery technology.

CHAPTER 5. BATTERY EVALUATION SYSTEM DESCRIPTION

A custom battery evaluation system was built in-house. National Instruments (NI) LabVIEW 8.5 software was used to create custom battery evaluation virtual instrument (VI) files for various battery related projects, such as pulse electroplating, material conductivity determination, battery charging/discharging, and battery cycling. The ease of the LabVIEW software allows one to very easily modify one VI file to make applicable to another technique or project.

A Dell Optiplex 760 personal computer (PC) was used as the processing unit for the laboratory evaluation system. The PC was equipped with a NI PCI-6229 data acquisition (DAQ) card. The DAQ card provides 2-way communication between the software and the actual evaluation system components. In the case of the flow battery evaluation system, the DAQ card provided two 5V digital output signals on demand to open/close the 2 relays (switches) and received and interpreted an analog input signal used to read the battery voltage. The DAQ card was connected to a NI SCB-68 shielded terminal block. This terminal block is where the input/output signal lines were physically wired into the evaluation system. A schematic of the entire battery evaluation system is shown below in Figure 5.1.

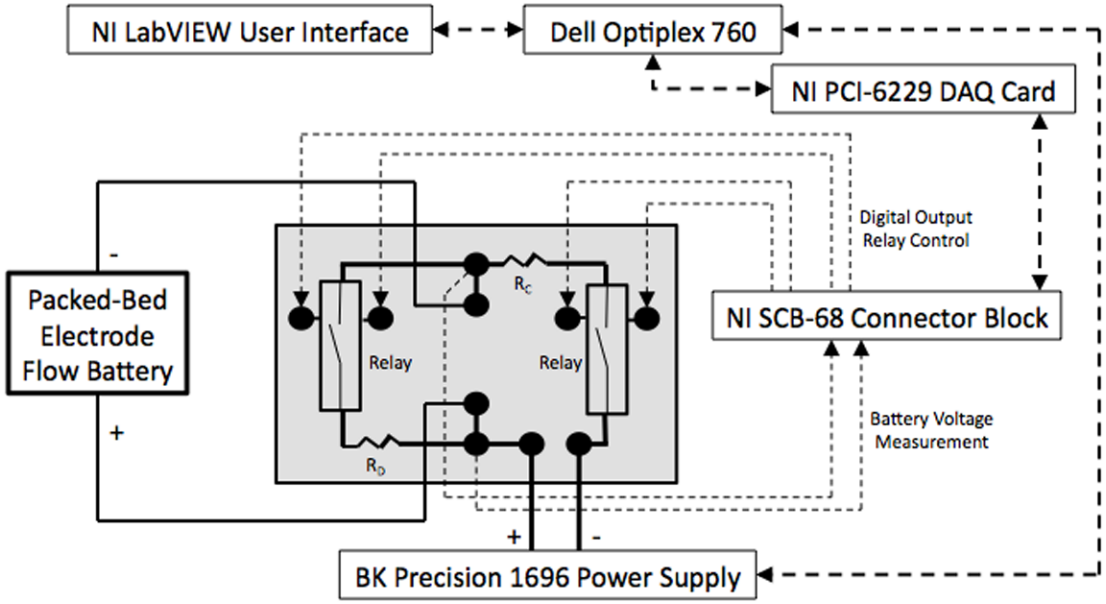

Figure 5.1. Schematic of battery evaluation system, signal lines are dashed and arrows indicate direction of the signal, double headed arrows indicate 2-way communication signals.

The circuit used for the evaluation system uses 2 relays that are used to route electric current through either the charging loop or the discharging loop of the circuit. The battery is connected in the center of the circuit board at the 2 innermost nodes. The charging loop is located on the right side of the circuit (gray box) pictured in Figure 5.1, and can be identified by the loop containing the attached battery, BK Precision 1696 power supply, relay, and a charge resistor (R_C). The discharging loop is located on the left side of the circuit in Figure 5.1, and can be identified by the attached battery, relay, and a discharge resistor (R_D).

The operation of the evaluation circuit is easy. The VI designed for charging/discharging was actually design to complete charge/discharge cycling on an

attached battery, but can be used for just charging or just discharging of a battery. By specifying the charge time duration, discharge time duration, charging voltage, and number of cycles the user can charge/discharge cycle the attached battery to their specifications. To charge an attached battery, a charge time duration and charging voltage is specified by the user (and by specifying zero for the discharge time duration and 1 for the number of cycles to complete) using the UI and the start button can then be pressed. The custom VI would then open the relay on the discharge side of the circuit, preventing current flow through the discharge resistor, and close the relay on the charge side of the circuit allowing current to pass through the charge resistor and begin charging the attached battery. For simplicity, the power supply was programmed to continually output a voltage and the application of that voltage to a connected battery was totally controlled by the charge side relay. To discharge an attached battery the VI performs opposite switching of the relays so that battery-sourced current is directed through the discharge resistance. The charge and discharge resistors can be switched by the user as they are just inserted into the terminals of the breadboard circuit.

CHAPTER 6. HIGH-ENERGY DENSITY FLOW BATTERY VALIDATION

The following manuscript was accepted for publication in the AIChE Journal on July 23, 2010 and can be located using the following information:

Suppes, G. J., Sawyer, B. D. and Gordon, M. J., High-energy density flow battery validation. AIChE Journal, n/a. doi: 10.1002/aic.12390

High-Energy Density Flow Battery Validation

Galen J. Suppes*, Bryan D. Sawyer, and Michael J. Gordon

Department of Chemical Engineering

University of Missouri

Columbia, MO 65211

*Email: suppesg@missouri.edu

*Phone: 573 447 1576

6.1 Abstract

A zinc-alkali flow cell was used to validate a new type of flow battery where all reagents and products remain as solids on the electrodes. In every case, flow of electrolyte reduced overpotential losses as compared to operation without electrolyte flow. Large separation distances between the electrodes resulting from larger sections of separating tubing led to increased overpotential losses. A mass transfer mechanism is proposed which substantiates increasing overpotential with increasing electrode separation distances. Based on this mechanism it was hypothesized that ion exchange packing would reduce the overpotential losses; this was experimentally validated.

Topical Heading: Environmental and Energy Engineering

Keywords: battery, flow, energy, packed bed electrode, electrolyte

6.2 Introduction

Most commercial batteries rely on diffusion of ions between electrodes to complete the circuit in sandwich-type battery configurations. To maximize diffusion, the electrodes are packed closely together with polymer, cellulose, or fiberglass separators inhibiting the direct contact (short circuit) of counter-electrodes. As a result, battery costs tend to be dominated by manufacturing and membrane costs that considerably exceed the cost of the active reagents[27, 62]. This paper describes the validation of a new type of flow battery that pumps electrolyte between reagents loaded in packed-bed electrodes separated by a permeable ion-exchange material.

The four basic components of a battery are 1) the anode where electron-generating half-reactions occur, 2) the cathode where electron-consuming reactions occur, 3) an electrically-conductive path from the anode to the cathode which does not conduct ions, and 4) an ion-conductive electrolyte between electrodes which does not conduct electrons. Figure 6.1 illustrates how these basic components can manifest into either a sandwich configuration designed to maximize diffusive mass transfer or a flow battery configuration with convective mass transfer.

The ion transport in most commercial batteries relies on bulk diffusion, which has the advantage of no moving parts. To maximize diffusion, these sandwich configuration designs use thin membranes and relatively thin electrode layers, such as in spiral designs[63]; and this introduces a variety of design constraints. For example, metallic lithium is not used in rechargeable batteries because the recharging of metallic lithium can lead to dendrite crystal growth which can traverse through the membrane

separator and short circuit the battery. The standard approach to avoid dendrite growth is to use a graphite support for lithium ions where the lithium exists in an intercalated state that has about 50 mV less potential than is needed to form dendrite crystals. The maximum loading of the intercalated lithium is 1:6 (moles, lithium:carbon). The result is that active chemical reagents, like lithium, often tend to be a minor component in a battery with the major costs being directly or indirectly related to design constraints associated with the need for high separator areas and thin electrodes—both employed to reduce diffusion overpotential.

The goal of this work is to validate a new type of flow battery that can be systematically used to reduce battery costs by reducing the use of separators and increasing the thicknesses of electrodes. The zinc alkali battery chemistry was used to test this new type of flow battery design, but it is applicable to other chemistries as well.

6.3 Background

The term "flow battery"[54, 64] traditionally refers to a class of batteries where at least one reactant or product is not a solid phase on an electrode and the flow of electrolyte facilitates the transfer of that reactant/product to the electrodes. A distinguishing feature of the flow battery is that at least one substrate (or product) is stored external to the electrode assemblies, typically in a tank of electrolyte. Flow batteries that have been extensively studied include those relying on soluble lead (in methanesulfonic acid)[50-52], soluble copper (as copper sulfate)[57], soluble zinc (in alkali water or as zinc chloride)[53-54], chlorine as liquid $SOCl_2$[65] , chlorine gas[66], and oxygen gas[67].

The redox (reduction-oxidation)[68] cell is a type of flow battery in which all reagents/products are stored in the electrolyte. In the redox cell, the electrodes serve only as an electrochemical reactor; the power output scales with the electrodes, while the stored energy is independent of the electrodes. Redox flow batteries can be rapidly recharged by refilling the tank with fresh electrolyte.

Flow batteries have a few major advantages over traditional diffusion based battery designs. For instance, higher power output is possible with the flow (reported to 500 mA/cm^2) of electrolyte when one of the reagents is stored in the electrolyte[65]. For these high power output batteries, the flow of electrolyte also facilitates heat removal. Elimination or substantial reduction of membrane separators is another advantage of flow batteries.

The proposed flow battery of this paper is different than traditional flow batteries since all reagents and products reside as solids, which are part of the electrodes. Ionic intermediates flow through the electrolyte but do not accumulate. An advantage of having solid reagents is that the activity of the reagents remains nearly constant during use whereas both the concentration and voltages from soluble reagents will decrease with use. Solid substrate batteries also tend to have higher energy densities due to a more-constant voltage output and the higher molar densities of pure solid reagents versus solvated reagents.

In the proposed flow battery shown in Figure 6.2, a pump circulates electrolyte between stacked electrodes. The goal is to pump ions between the electrodes at mass

transfer rates greater than is possible with diffusion alone. The distances between electrodes in this design can be increased from microns to millimeters, and even up to centimeters. Zhang et al report that dendrite growth is substantially absent when plating zinc in a flow battery.[54] When dendrite growth is not inhibited by the flow or control of flow, the flow battery creates the opportunity to increase separation of distances between electrodes to the point where dendrite modes of failure can be substantially eliminated. In sandwich cell configurations, separation distances created by separators are typically less than 50 microns, and these short distances are easily traversed by dendrite crystal growth. The dendrite mode of failure would be much easier to control (e.g. with electrolyte flow or pulse charging) with separation distances of 1000 microns or more.

For small batteries the diffusion-based architectures are superior because the cost of the circulating pump, alone, would be more than the cost of the traditional diffusion-based battery. However, for larger batteries the savings in separator and cathode intercalation material costs can more than offset the cost of a pump. Typical applications of the convection battery would be plug-in hybrid electric vehicles and electric grid energy storage.

This paper is on the validation of the flow battery and includes the identification of key overpotential losses of rudimentary flow battery designs. Approaches are demonstrated that overcome the major overpotentials of the rudimentary designs. The purpose of this work is to evaluate the impact of materials and architectures of this

novel flow battery on performance. At this point in research, battery cycling studies are not needed and were not performed.

6.4 Experimental

Two types of flow cell designs were used in these validation studies. One design (Figure 6.3) is ideal for evaluating relatively large electrode separation distances, while the other design (Figure 6.2) is a more practical flow battery design. Both of these designs incorporate packed beds of electrochemical active materials as the anode and cathode and both designs utilize tubular stainless steel current collectors at the anode and cathode

6.4.1 Electrode Separation Distance

Figure 6.3 is a schematic of the flow cell design in which separation distances between 2.5 cm and 43 cm were evaluated. The anode and cathode assemblies are separate stainless steel cylinders, each with a precision-machined stainless steel piston equipped with an o-ring seal that allows for material compression and current collection. Each electrode assembly has an electrolyte inlet through the wall of the cylinder near the base and an electrolyte exit, which is on the opposite side of the cylinder from the inlet, near the top. This arrangement ensures that flow is directed through the entire packed electrode bed. Nylon hose barbs were attached to inlet and exit ports of the anode and cathode assemblies to facilitate the use of laboratory tubing connections between the electrodes. Different lengths of Masterflex Norprene

peristaltic pump hose (Cole-Parmer) were used to separate the anode and cathode assemblies.

In the evaluation of electrode separation distance effects on the flow battery, granular zinc (99.8%, 110-50 mesh, ACS reagent grade, Sigma Aldrich) was used as the anode active material, while two different cathode compositions were used. The first cathode composition consisted of cathode materials harvested from a Duracell Procell alkali battery. This material is believed to contain binder, which upon compression was hypothesized to hinder flow through material, therefore this material was combined with stainless steel wool (Briwax Online) and stainless steel shot (0.4mm, Pellets, LLC) to increase bed permeability. The second cathode composition consisted of 25 wt.% manganese (IV) oxide (60-230 mesh, ≥99%, Sigma Aldrich) as active material and 75 wt.% graphite (approximately 0.2mm, Sigma Aldrich) as a bed conductivity enhancer. A two molar potassium hydroxide (≥90%, reagent grade, Sigma Aldrich) in distilled water solution was used as the electrolyte.

Cell assembly began by loading glass wool into the hose barbs to prevent materials from being carried away by electrolyte flow. The electrode materials were then mixed and loaded into their respective cylinders and pistons were then inserted into the cylinders. Masses of approximately 5.6 kg were loaded onto each piston to ensure packed bed compaction. Circulation tubes were then connected to electrode assemblies and feed and discharge lines were inserted into the electrolyte reservoir.

The feed line was then inserted and secured into a Masterflex Easy Load II L/S pump head driven by a Masterflex console pump drive, and electrolyte flow was initiated.

The flow batteries with 2.5, 13, 23, 33, and 43 cm separation distances were each subjected to a 550-ohm external load, and cell potentials were recorded as a function of time using a personal computer equipped with a National Instruments PCI-6024E data acquisition card connected to a National Instruments SCB-68 shielded I/O connector block. A custom LabVIEW virtual instrument (VI) file served as the graphical user interface for data acquisition. Once leads from the connector block were connected to the electrode pistons, data acquisition could be initiated. Once started, the LabVIEW VI simultaneously sends a signal to close the external circuit (through use of a relay) and begins recording data. Once the user defined discharge time elapses the VI opens the external circuit and stops data acquisition.

6.4.2 Electrolyte Flow vs. No Flow

Electrolyte flow studies were conducted in a stacked packed bed arrangement as shown in Figure 6.2. Sections of 2.5 cm long and 1.25 cm outside diameter stainless steel tube were used as the anode and cathode current collectors. These anode and cathode sections were joined with a custom machined high-density polyethylene (HDPE) coupling equipped with o-ring seals to form a liquid tight seal around the inserted electrode current collectors. A non-conductive HDPE top piece was custom machined to act as both a piston for transferring pressure to packed beds and as an electrolyte outlet, as it was tapped and fitted with a nylon hose barb. A HDPE bottom piece was

machined similar to the coupling with an o-ring seal to seal around the inserted anode current collector and tapped and fitted with a nylon hose barb to provide an electrolyte inlet. Similar to the electrode separation distance experiments, granular zinc was used as the anode material in the electrolyte flow study. A 30 wt.% manganese (IV) oxide, 35 wt.% graphite, and 35 wt.% ALL-CRAFT 4K activated carbon (US Patent Publication 20080207442) mixture was used as the cathode mixture. Electrolyte mixtures of 2, 3, and 4 molar potassium hydroxide in distilled water were used in these studies.

Cell assembly began by placing a 1.25 cm diameter piece of Fisherbrand P8 filter paper (Fischer Scientific) inside the HDPE bottom cell piece, beyond the o-ring seal until is rested against the bottom. The stainless steel anode current collector was then rotated and pressed into the bottom HDPE piece by hand until visual inspection revealed it was completely inserted. Granular zinc was then added into the anode current collector and compacted by hand using a stainless steel rod. Once anode collector was full of zinc, three 1.25 cm diameter pieces of filter paper were inserted into one side of the HDPE coupling. Care was taken to make sure filter paper remained un-creased and that it was seated against the center lip inside the coupling. The side of the coupling that the filter paper was inserted into was then rotated and pressed over the full anode collector until it was firmly seated over the collector. The cathode current collector was then inserted into the other side of the coupling and visual inspection was used to make sure it was firmly seated on the center lip of the coupling. Cathode mixture was then added a little at a time with light hand compression after each addition of material. Once all of the cathode mixture was added, the outlet at the

tip of the HDPE piston was covered with two wetted 0.95 cm diameter pieces of filter paper to prevent loss of active material, and then the piston was inserted into the cathode current collector to complete the cell assembly. The cell was then loaded into a small hydraulic press and Masterflex peristaltic pump hose was used to connect the electrolyte inlet and outlet to the electrolyte reservoir. The feed line was then inserted into the pump head and electrolyte flow was initiated.

Flow cells using each electrolyte concentration were subjected to a 550-ohm external load for 20 minutes with electrolyte flow, then the flow was ceased for 20 minutes, and then flow was resumed for 20 minutes. Also, 30 minute discharges (550-ohm) with and without 2M potassium hydroxide flow were conducted to directly compare differences in their voltage profiles. The same data acquisition system discussed previously was used for these experiments.

6.4.3 Ion Exchange Material

A stacked packed bed cell similar to that used in the electrolyte flow study (Figure 6.2) was used to evaluate the effects of the addition an ion exchange resin between the anode and that cathode. The only difference to the cell used for this study is that an additional 2.5 cm long and 1.25 cm diameter stainless steel cylinder and an additional HDPE coupling were used to accommodate the addition of the ion exchange resin. Granular zinc was used as the anode material and a mixture of 30 wt.% manganese (IV) oxide, 35 wt.% graphite, and 35 wt.% ALL-CRAFT 4K activated carbon was used for the cathode mixture. A two molar potassium hydroxide in distilled water

solution was used as the electrolyte in this study. All assembly steps remained the same as electrolyte flow study except for the addition of a third middle section that was hand packed full of Amberlyst A-26(OH) (Sigma Aldrich) strongly basic ion exchange resin. Again, the cells were subjected to a 550-ohm external load and a PC and National Instruments hardware and software were used for data acquisition.

6.5 Results and Discussion

6.5.1 Electrolyte Flow vs. No Flow

Three electrolyte concentrations (2M, 3M, 4M KOH) were used in an alternating flow:no-flow:flow scheme to determine the magnitude of overpotentials associated with electrolyte flow and to understand how the cell rebounds after electrolyte flow is restored. It was hypothesized that higher concentrated electrolytes would benefit by having a larger number of anions locally present at electrodes when electrolyte flow was ceased.

Figure 6.4 illustrates the impact of stopping electrolyte flow and how the differences in electrolyte molarity effect flow battery performance. After stopping electrolyte flow, the voltage profiles remain unchanged for a small amount of time before an increase in the rate of voltage loss occurs. The increase in the rate of voltage loss is due to the continuous consumption of OH^- (reactive ion) ions locally present in the anode at the instance flow is stopped and also to an accumulation of OH^- ions in the cathode as they are produced. The accumulation of OH^- ions in the cathode has a negative effect on the cathode reaction kinetics, which leads to a negative effect on the

cell potential. After restarting electrolyte flow, the cell voltage rebounds back to a value similar to that before electrolyte flow was turned off. This occurs because of the replenishment of OH^- ions in the anode and the removal of the accumulated OH^- ions in the cathode allow the electrochemical reactions to proceed with more favorable kinetics, and therefore a higher cell potential.

It is also evident by Figure 6.4 that higher concentration electrolytes allow the flow cell to operate at higher voltages for longer periods of time without electrolyte flow. This is due to higher concentration electrolytes providing larger reservoirs of reactive OH^- ions at the time electrolyte flow is stopped. With more OH^- ions locally available, the concentration driving force is sustained longer allowing the flow cell to retain a higher voltage longer.

A simple comparison of discharge runs with and without flow of a 2M potassium hydroxide is shown in Figure 6.5. Despite a low current draw (550-ohm) from the flow cell, Figure 6.5 shows there is about a 48 mV difference, after 30 minutes of discharge, between discharge runs with and without electrolyte flow. A higher discharge rate would be suspected to increase this voltage separation at the 30 minute mark.

6.5.2 Electrode Separation Distance

A goal of the convection battery design is to separate the electrodes by a sufficiently large distance so as to eliminate dendrite modes of battery failure. Figure 6.6 summarizes the impact of separation distance between the electrodes on the operating voltage of the cell. Shorter separation distances exhibited higher operating

voltages. A hypothesis, which explains this behavior, is that the flow of electrolyte provides the desired transfer of the OH^- anion for the zinc-alkali battery; however, the flow introduces a new need for counter-diffusion of the K^+ counter-ion. The need for counter-ion diffusion and associated effects would only become stronger with increased separation distances between the anode and cathode, as the counter-ions would need to diffuse a greater distance against convective electrolyte flow and this is confirmed by the trend shown in Figure 6.6.

Figure 6.7A illustrates the mass transfer mechanism associated with a diffusion based battery where the electrolyte is stagnant, so the K^+ ions are non-mobile and able to stabilize the concentration driven (as result of electrochemical reaction) diffusion of the OH^- ions. Figure 6.7B depicts the hypothesized mechanism occurring in a flow cell, where the electrolyte is flowing from cathode to anode. Immediately leaving the cathode, the electrolyte is unstable due to a local excess of OH^- ions. To stabilize the transport of OH^- ions, K^+ ions must counter-diffuse to balance the charge of the excess OH^- ions. This situation creates a transport-based overpotential. It is hypothesized that this overpotential can be reduced by the use of a cationic ion exchange resin between the cathode and anode that would provide stability to the excess OH^- ions being transported.

6.5.3 Ion Exchange Material

A hypothesized approach to overcome the counter-ion counter-diffusion problem when flowing from a cathode to anode is to use an ion exchange resin that has

a fixed cationic charge to provide stability for the transport of excess anions in solution. Figure 6.7C illustrates this proposed mechanism by using an ion exchange resin with a fixed cationic charge to stabilize the excess OH^- being transported between the cathode and anode.

With electrolyte flowing from anode to cathode, an improvement in performance (Figure 6.8) was attained with the addition of Amberlyst A-26(OH) anionic ion exchange resin between the electrodes (fixed anionic charge to stabilize a local excess of K^+ ions being transported from anode to cathode). Amberlyst A-26(OH) reduced the overpotential by about 80 mV and kept the useable potential well above 1 V. This improvement indicates a more efficient (less overpotential loss) use of the active materials by allowing the cell to operate at higher voltages for a longer period of time.

Figure 6.7C illustrates the interesting concept of sustaining an electrolyte flow where the electrolyte has a net negative charge. This configuration illustrates the approach to literally pump anions (without counter-ions) from the cathode to the anode. As summarized by the anodic half-reaction for this zinc-alkaline battery (Equation 6.1), the hydroxide anions are the reactive ion and the potassium cations are only necessary to stabilize the hydroxide ions in solution.

$$Zn + 2OH^- \ <=> ZnO + \ H_2O + 2e^- \qquad (6.1)$$

As the flowing electrolyte leaves the anode it has a net positive charge, which would represent a high energy and unstable state that would ultimately limit the ability to pump anions from the cathode to the anode. The energy state of this fluid leaving the

anode must be reduced for the flow battery to reach its potential. Figure 6.9 illustrates a configuration that would reduce the energy state through use of a second bed of ion exchange resin.

Through the use of two ion exchange resin sections between three electrodes, a net anion flow from the first cathode to the anode is balanced by a net cation flow from the anode to the second cathode. The electrolyte leaving the second cathode has zero net charge, and the electrolyte half way through the depth of the anode will have a net zero charge.

These results are with an off-the-shelf ion exchange resin consistent with what is used in ion exchange chromatography. Ion exchange materials specifically designed and fabricated for this application would be expected to improve performance.

The traditional diffusion overpotential loss term is more accurately described as mass transfer overpotential for the system of Figure 6.9. The mass transfer overpotential has contributions from: ion convection, counter-ion counter diffusion, and boundary layer diffusion from the flowing electrolyte to the surfaces of the electrodes.

Ion convection overpotential losses can be made negligible by increasing the electrolyte flow rate. Electrolyte flow rates for these studies varied between 400 and 850 times what was required by stoichiometry of the electrochemical reactions. As the electrolyte flows through the packed bed, it will become depleted in the reactive ion. Thinner electrodes will also decrease these losses.

Counter-ion counter-diffusion overpotential losses can be reduced through the development of ion exchange materials that are able to effectively stabilize ions being transported between the electrodes. Equally important will be the use of ion exchange materials in the packed beds. The maximum power output per cross sectional area (perpendicular to flow) will be limited by the performance of this ion exchange media. When operating at high power output where the capabilities of the ion exchange material are reached it is expected that the voltage of the cell versus the electrolyte flow rate will have a maximum. At lower flow rates, the convection of the ions is not adequate to meet power requirements while at higher flow rates counter-ion counter-diffusion will be required as the capacity of the ion exchange material is exceeded.

Boundary layer diffusion overpotential losses can be reduced by increasing the boundary layer surface area and by increasing the specific active surface area of the particles. Smaller particles will decrease this overpotential, but only at the expense of increasing pressure drops for flow through the packed beds. There will always be an optimal permeability, which can be related to particle size distributions, that balances boundary layer diffusion overpotential with pressure drop for flow through the bed. Ultra-high surface area mesoporous carbons (>3,000 m^2/g) carbons will reduce these diffusion overpotential losses. These same carbons may also provide ion exchange capacity in the packed beds.

The ability to which these three overpotential losses can be overcome to achieve higher levels of charge flux for pumping anions/cations between electrodes is an

unexplored area of science with immediate application. The flow battery design overcomes the traditional battery design paradigm where increased power in a battery has been at the expense of decreasing the energy density and increasing the battery costs (more membrane area and thinner electrodes). When the ability to pump anions and cations between electrodes is combined with ultra-high surface area carbons, it may be possible to create low cost batteries that can provide 320 kilometers of travel in electric vehicles and be charged in times comparable to the time it takes to refuel with gasoline.

6.6 Conclusions

A new type of flow battery has been validated where all reagents and products remain as solids on the electrodes. This flow battery has the potential to gain higher energy densities than other types of flow batteries and provides an excellent platform for rechargeable lithium batteries that allow use of metallic lithium in the anode. An approach incorporating a permeable ion exchange material between electrodes was validated and is hypothesized to be a key aspect of this flow battery design to maximize the power output per area of separator between electrodes.

6.7 Acknowledgements

A special thanks is extended to the National Science Foundation (Award 0940720) and the following graduate and undergraduate co-researchers: Alex R. Hunter, Eric Leimkuehler, Eric M. Nordwald, Ashley N. Ulrich, Matt Wavada, and Matthias Young.

6.8 List of Figures

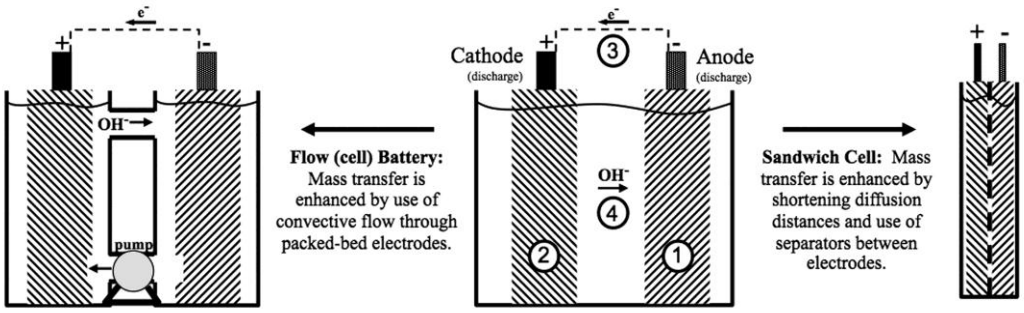

Figure 6.1. Schematic of a battery illustrating components with four basic functions (1-anode, 2-cathode, 3-electron transport, 4-ion transport) and the transformation of these basic components into the sandwich cell for diffusive mass transfer and the flow cell for convective mass transfer.

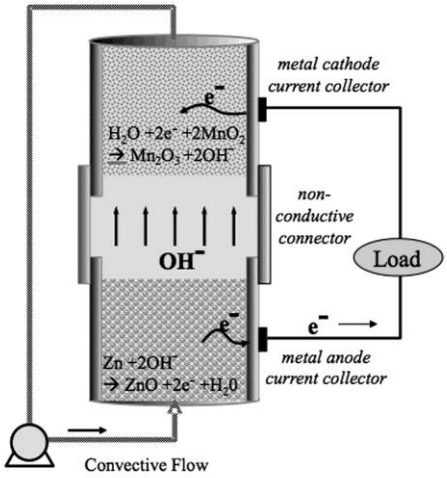

Figure 6.2. Schematic of stacked electrode flow cell that utilizes packed bed electrodes with tubular stainless steel current collectors separated by a non-conductive coupling.

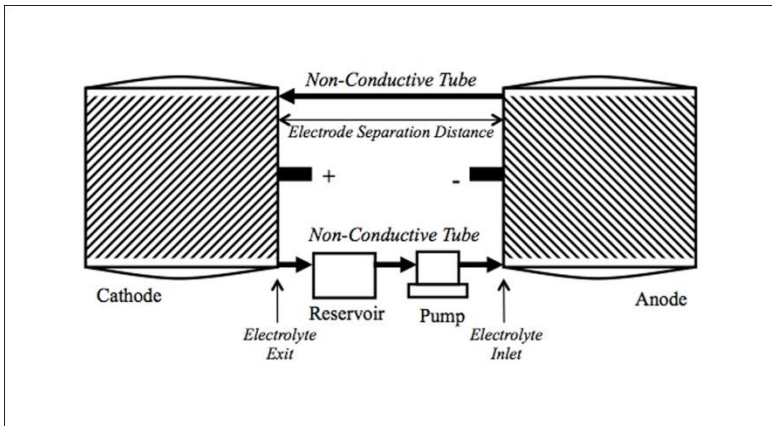

Figure 6.3. Schematic of flow cell comprised of separate packed bed electrodes with stainless steel cylindrical current collectors separated by non-conductive tubing.

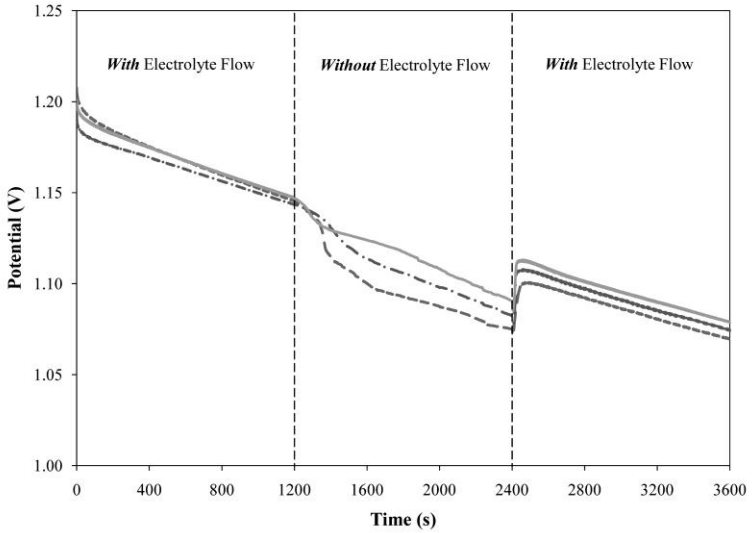

Figure 6.4. Electrolyte flow effects on stacked flow cell potential under a 550-ohm load at 3 different electrolyte concentrations, 4M KOH-solid line, 3M KOH-dash dot line, 2M KOH-dashed line.

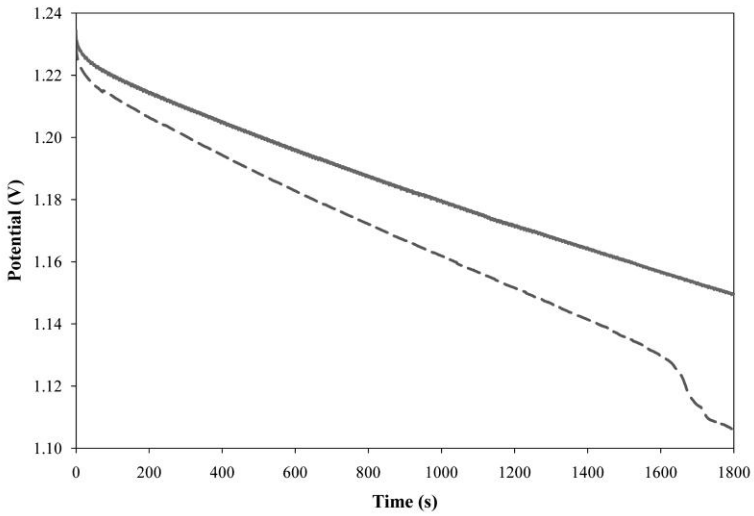

Figure 6.5. 30 minute discharge at 550-ohm with (solid) and without electrolyte flow (dashed) using 2M KOH electrolyte.

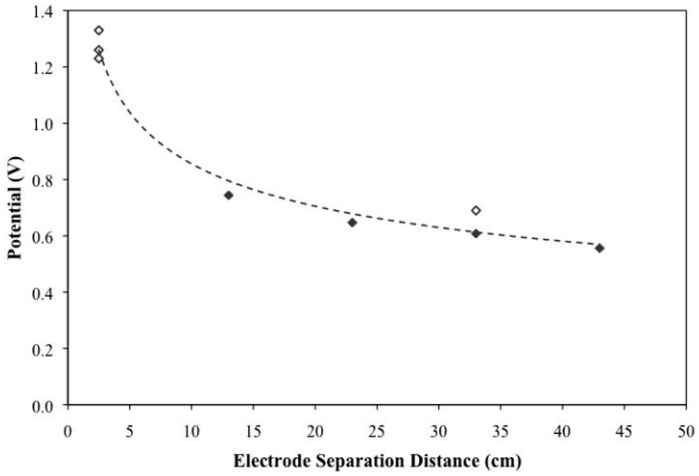

Figure 6.6. Electrode separation distance effects on flow cell closed circuit potential. Hollow diamonds indicate flow cell with harvested cathode from Duracell Procell alkaline battery mixed with stainless steel wool and shot, and solid diamonds indicate flow cell with cathode composition of 25 wt.% manganese (IV) oxide and 75 wt.% graphite.

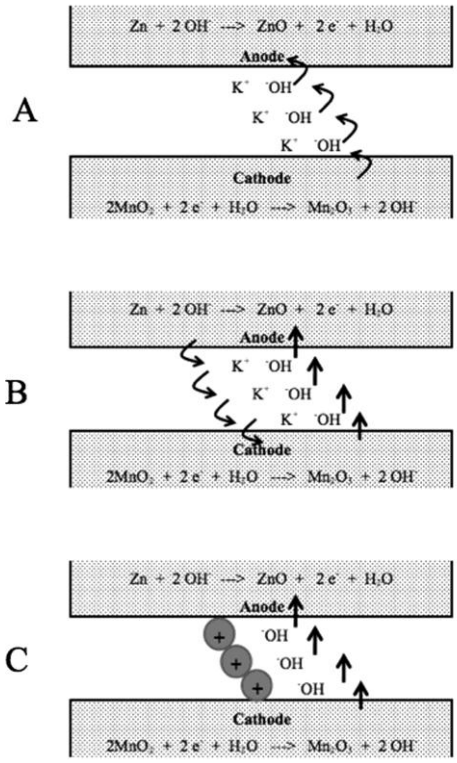

Figure 6.7. Illustration of mass transfer of hydroxide ions with three different approaches: A. sandwich configuration (diffusion) cell, B. convection battery where the material of the spacer does not interact with the ions, and C. convection battery with non-conductive cation exchange material between the electrodes. The cation exchange material improves performance by reducing the need for counter-ion counter-diffusion.

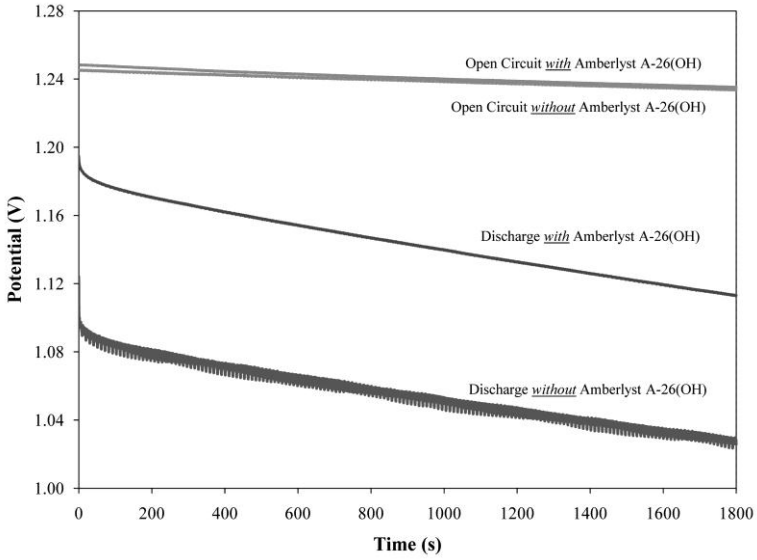

Figure 6.8. Comparison of flow cell performance under 550-ohm load with and without Amberlyst A-26(OH) anionic ion exchange material between electrodes.

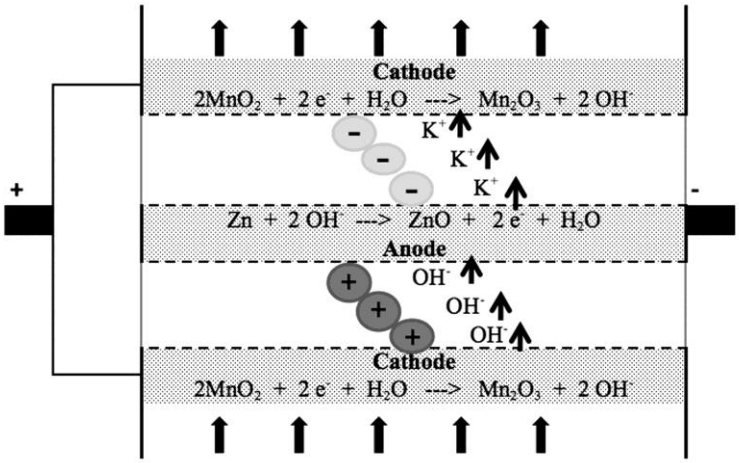

Figure 6.9. Illustration of flow cell electrode configuration designed to stabilize the flow of electrolyte with net charges.

CHAPTER 7. IMPACT OF ELECTRODE SEPARATOR ON PERFORMANCE

The following manuscript was submitted to the Journal of Applied Electrochemistry on October 22, 2010 to be considered for publication and is currently under consideration.

Impact of Electrode Separator on Performance

Bryan D. Sawyer, Galen J. Suppes*, Michael J. Gordon, and Michael G. Heidlage

Department of Chemical Engineering
University of Missouri
Columbia, MO 65211

*Email: suppesg@missouri.edu
*Phone: 573-447-1576

7.1 Abstract

A zinc/alkaline/manganese dioxide packed-bed electrode flow battery was used to evaluate using granular materials with ionic activity as separating materials between electrodes, increasing the separation distance between electrodes while using separating materials, and reversing the electrolyte flow direction through the flow battery. Results indicate that materials with more ionic activity (ion exchange resins) perform better than materials with limited ionic activity (stainless steel). Among the more ionically active materials, the basic material out-performed the acidic material with an anode-to-cathode flow regime at low current draw. The best performance was obtained using ALL-CRAFT 4K activated carbon as separation material. The use of an ionically active separation material reduced the difference in cell performance between 2.22 cm and 5.40 cm of separation by 56%. Although expected to be an important parameter for packed-bed electrode flow battery, the electrolyte flow direction did not produce a discernable difference in performance using the low current draw of these studies.

Keywords: battery, flow, energy, packed-bed electrode, electrolyte, separator

7.2 Introduction

As more of the world progresses away from the complete use of liquid fossil fuel and advances toward the use of plug-in hybrid electric vehicle (PHEV) technologies for transportation use, there will be a high demand for larger scale, higher energy density electrical energy storage devices. These large-scale devices will also play a vital role in the sustainability of a renewable energy power grid by serving as point-of-source storage for excess electricity produced during off-peak periods. At times of peak electricity usage, the large storage devices will provide supplemental power to the power grid. The large-scale electrical energy storage devices will also benefit the renewable energy power grid by being able to efficiently store renewable electricity during intermittent times of high renewable electricity production by wind turbines and photovoltaic devices.

Current state-of-the-art battery systems, such as lithium-ion technology, are relatively expensive and have just recently been implemented for transportation use. Lithium-ion batteries use a specialized polymer separator to prevent electrical contact between the anode and cathode while still allowing for lithium-ion diffusion between the electrodes. The design and optimization of these separating materials is a science of its own and is continuously pursued by the battery industry to produce more efficient and safer batteries. The time and engineering applied to these separators lead to increased battery costs.

Cathode intercalation materials of the lithium-ion battery are also expensive. These materials are designed for reversible lithium-ion insertion (without reduction of

the lithium ion) into the voids of their crystal structure. The cost of these cathode intercalation materials ranges depending on the metal being used in the material. Again, the time and engineering required for the optimization and development of these cathode intercalation materials drives up the cost of the final lithium-ion battery.

All conventional battery systems rely on bulk diffusion of ions between the anode and the cathode for operation. Years of development have led to battery designs with very thin layers of active materials at each electrode separated by very thin separators to minimize diffusion distances, which have a positive impact on battery performance. The manufacturing of thin electrodes with thin layers of active materials coated on thin metal current collectors requires precision. The equipment and processing required for thin coating production lead to increased manufacturing costs, which ultimately increase final battery costs.

The costs associated with conventional diffusion based battery technologies are acceptable for use in everyday items such as cell phones, laptop computers, and digital music players, but when the energy requirements are several magnitudes larger these costs can be problematic. A new design for large-scale electrical energy storage devices is needed to reduce total costs to make extreme scale-up economically feasible.

A new battery design will need to meet a long list of criteria to prove itself eligible for worldwide deployment. Such important criteria are high energy density, long cycle life, scalability (above a minimum threshold scale), high material utilization efficiency, deep cycle ability, applicability to various electrochemistries, and improved

safety. It is also very important for the new battery design to be dominated by the cost of the electrochemically active components as opposed to highly engineered battery structure components.

In previous work, a validation of a packed-bed electrode zinc/alkaline/manganese dioxide battery with flowing electrolyte was discussed.[69] It was determined that increasing the separation between the anode and cathode had a negative impact on the cell potential, electrolyte flow had a positive impact on the cell potential, and that the presence of a strongly basic ion exchange resin between the anode and cathode had a positive impact on the cell potential. Based on these previous results, the goal of the present work was to explore the use of other materials between the anode and cathode, impact of electrode separation distance in the presence of the materials between electrodes, and the impact of electrolyte flow direction (anode-to-cathode, cathode-to-anode) in the presence of the materials between electrodes. The present work is applied to the zinc/alkaline/manganese dioxide battery chemistry, but it is important to understand that this design can be employed to other electrochemistries.

7.3 Background

The term "flow battery"[54, 64] typically refers to electrochemical cells in which at least one of the active materials exists in a mobile phase. The operation of the flow battery requires the mobile active phase to circulate through the flow battery. Circulation of a mobile phase has the advantage of removing heat from the flow battery and, in cases where at least one active material is in the mobile phase, higher power

output can be obtained by increasing the flow rate. A major advantage of the flow battery architectures is that money is saved through the elimination or reduction in size of needed separation membranes. There has been an abundance of previous research on flow batteries. Different flow battery architectures have been applied to numerous electrochemistries that employ soluble lead[50-52], soluble copper[57], soluble zinc[53-54], thionyl chloride (liquid)[65] , chlorine gas[66], and oxygen gas[67] as active components.

A distinction of the flow battery of the present work is that all active materials exist and remain in a solid state in the packed-bed electrodes. The circulation of the electrolyte allows for the transfer of ionic intermediates between the electrodes to allow for the electrochemical reactions to proceed. A major advantage of solid active materials is that the activities of the materials remain nearly constant throughout use whereas both concentration and voltages from soluble active materials decrease during use. Batteries employing solid active materials tend to have higher energy densities due to a more constant operating voltage and higher molar densities of pure solid active materials versus solvated active materials.

In the flow battery of the present work (Figure 7.1), a pump circulates electrolyte between stacked electrodes. The goal is to pump ions between the electrodes at mass transfer rates greater than is possible with diffusion alone. The distances between electrodes in this specific design can be increased from 2.2 cm to any practical length. In conventional battery designs the electrodes are only separated by separator materials typically less than 50 microns thick. These short separation distances are

easily traversed by dendrites that form when recharging metallic anodes and that is why most metallic anode batteries are not rechargeable. It is a benefit of the flow battery of the present work to separate the electrodes by relatively large distances to eliminate the possibility of a dendrite induced short circuit, if in any case the dendrite formation cannot be controlled by the flow or control of flow of the electrolyte.

For small portable batteries the diffusion-based architectures are superior, as the cost of the circulating pump would cost more than the traditional diffusion-based battery. However, for larger batteries the savings in large areas of required separation can more than offset the cost of a pump. The higher active material to separating material (granular, not in sheet form) ratio of the packed-bed electrode flow battery makes it more economical for large-scale electrical energy storage needs. Typical applications of the packed-bed electrode flow battery would be plug-in hybrid electric vehicles and point-of-source electrical energy storage for load leveling applications.

The present work is a discussion of the effects of using separation materials with different ionic behavior between the anode and cathode, the impact of separation distance in the presence of separation materials, and the effects of electrolyte flow direction on a packed-bed flow battery with all active materials in solid form.

7.4 Experimental

The packed-bed electrode flow cell used in these studies is shown in Figure 7.2. It consists of a high-density polyethylene (HDPE) base fitted with a nylon hose barb to facilitate electrolyte entry/exit, 1.27 cm outside diameter stainless steel tubes for anode

and cathode current collection (also used for separation material section), HDPE separation couplings to maintain electrical isolation between the anode, cathode, and separation material sections, and a stainless steel piston (that slides into top electrode tube) top fitted with a nylon hose barb to facilitate electrolyte entry/exit. This piston top allows for compression to be applied to the packed electrode beds (using a small hydraulic press).

The flow cell was assembled from the bottom to the top. A single piece of Fisherbrand P8 filter paper punched into a circle with a 1.27 cm diameter was placed into the bottom the bottom HDPE piece to prevent material from being lost in the electrolyte entry/exit port. The anode collector tube was then inserted into the bottom HDPE piece by rotating and pressing it passed the o-ring seal until it was seated tightly against the filter paper in the bottom of the HDPE bottom piece. Granular zinc (99.8%, 110-50 mesh, ACS reagent grade, Sigma Aldrich) was then added into the anode current collector tube and hand packed until the zinc was level with the top of the anode collector tube. Then, a single piece of P8 filter paper punched to 1.27 cm in diameter was inserted into one side of a HDPE coupling until it rests evenly against the lip in the middle of the coupling. This side of the coupling containing the filter paper was then rotated and pressed over the end of the anode tube until the anode tube was passed the o-ring seal and seated firmly against the filter paper and coupling lip. The separating material stainless steel tube was then pressed and rotated into the top of the HDPE coupling that was just attached to the anode, and separating material (separation materials were varied and will be detailed in specific subsections) was added and hand

packed until the material was level with the top of the separating material tube. Like before a piece of 1.27 cm diameter filter paper was inserted into the remaining HDPE coupling and the coupling was positioned onto the top of the separating material tube. The cathode current collection tube was then inserted into the top of the second HDPE coupling and the cathode material mixture consisting of 30 wt.% manganese (IV) oxide (60-230 mesh, ≥ 99%, Sigma Aldrich), 35 wt.% graphite (Sigma Aldrich), and 35 wt.% 4K activated carbon[70] was loaded and hand packed into the tube (the cathode tube is never filled completely because room is needed for the piston). Finally, the stainless steel piston (equipped with an o-ring seal) was inserted into the cathode current collection tube. Once fully assembled, the cell was placed in a small hydraulic press and enough pressure was applied to hold the cell in place while electrolyte feed/discharge hoses are attached to the hose barbs of the cell. A two molar potassium hydroxide (≥ 90%, reagent grade, Sigma Aldrich) solution (in distilled water) was used as the electrolyte and was circulated through the flow cell using Masterflex Norprene peristaltic pump hose (Cole Parmer) and a Masterflex Easy Load II L/S pump head (Cole-Parmer) driven by a Masterflex console pump drive (Cole-Parmer). The electrolyte was pumped from a 60-mL reservoir and returned to the same reservoir upon exiting the flow cell for recirculation.

The flow cells were assembled as described above and were then connected to an external discharge circuit with switch automation for opening and closing the circuit. Voltage measurement and automated switch signals were provided by National Instruments LabVIEW software (using custom created virtual instrument files) through a

National Instruments PCI-6229 data acquisition card connected to a National Instruments SCB-68 shielded connector block.

For all of the studies of the present work, the flow cells were first subjected to a 45-minute start-up period where electrolyte flow was initiated and allowed to reach a steady state. Near the end of this start-up period, the electrolyte flow rate through the flow cell was determined. Immediately following the start-up period, the flow cell was operated for 30-minute open circuit period. After the open circuit period, the flow cell was discharged through a 550-ohm load for 30 minutes to obtain voltage profiles used in the analysis.

7.4.1 Survey of Separating Materials

Previous work indicated that the addition of an anionic ion exchange material into the tubular space between the anode and cathode increased the operating potential of the flow cell when compared to a stainless steel shot (0.4 mm, Pellets, LLC) control. In the present study, a survey of materials with varying ionic properties were evaluated as separating materials between the anode and the cathode to determine effects on the operating cell potential. A 2.54 cm long stainless steel tube was used as a tubular separator between the anode and cathode and was filled with separating materials to be studied. The anode and cathode materials used are discussed above and the separating materials evaluated were Amberlyst A-26(OH) strongly basic ion exchange resin (Sigma Aldrich), Amberlite IR-120H (Sigma Aldrich) strongly acidic ion

exchange resin, ethylene-acrylic acid copolymer beads (Allied-Signal, Inc.), stainless steel shot (0.4 mm, Pellets, LLC), and ALL-CRAFT 4K activated carbon[70].

7.4.2 Impact of Separation Distance in Presence of Separation Materials

It was determined in previous work that separation distance (in absence of separation materials) between the anode and cathode strongly affected the cell potential. It was determined that greater separation distances resulted in increasingly negative impacts on flow cell potential. The present study is to determine the effects of electrode separation distance in the presence of separation materials.

The anode and cathode materials were the same as discussed above and only two separation materials were chosen for use in this study; Amberlyst A-26(OH) strongly basic ion exchange resin and stainless steel shot. The lengths of the middle separation tubes were varied to provide separation distances of 2.2-cm, 2.8-cm, 4.1-cm, and 5.4-cm between the anode and cathode.

7.4.3 Impact of Electrolyte Flow Direction

The operation of a zinc/alkaline/manganese dioxide cell relies on the transportation of hydroxide ions between the anode and cathode. Hydroxide ions are consumed at the anode during discharge as shown in the half-cell reaction of Equation 7.1. Hydroxide ions are produced in the cathode during discharge as shown in Equation 7.2.

$$Zn + 2OH^- <=> ZnO + H_2O + 2e^- \quad (7.1)$$

$$2MnO_2 + H_2O + 2e^- <=> Mn_2O_3 + 2OH^- \quad (7.2)$$

The electrolyte flow was directed from anode to cathode and then from cathode to anode using both the Amberlyst A-26(OH) strongly basic ion exchange resin and the Amberlite IR-120H strongly acidic ion exchange resin as separation materials in a 2.5 cm long stainless steel middle section of tubing. Based on the electrochemistry, it is hypothesized that electrolyte flow direction will have an impact on the operating potential of the flow cell due possible differences in electrolyte charge balancing mechanisms. Figure 7.3 provides a visual representation of the concentration changes associated with a change in flow direction. Charges in the electrolyte must remain balanced so increases and decreases in the OH^- concentration must be paralleled with increases and decreases in K^+ concentration.

7.5 Results and Discussion

7.5.1 Survey of Separating Materials

Figure 7.4 shows the impact of using materials with different ionic activity as the separating material between the anode and cathode. Initially, an 80mV increase in operating potential, after a 30 minute discharge through a 550-ohm load, was attributed to using Amberlyst A-26(OH) strongly basic ion exchange resin as the separating material in comparison with using stainless steel shot. Stainless steel was assumed to have very little ionic activity as it is designed to be a corrosion resistant material. Ethylene-acrylic acid copolymer beads were also assumed to have negligible ionic

activity with the electrolyte and indeed the cell performance using copolymer beads was very similar to the flow cell performance using stainless steel shot. This similarity can be seen in Figure 7.4.

The voltage profiles shown in Figure 7.4 were recorded as the electrolyte was circulated from the anode to the cathode. With OH^- ions being consumed in the anodic reaction (Equation 7.1), there is a slight decrease in OH^- concentration in the separating section between the anode and cathode. (See Figure 7.3) The decrease in OH^- ion concentration must be accompanied by a decrease in K^+ ion concentration. Since the K^+ ions do not participate in any reactions the concentration can only be reduced by the transfer of K^+ ions away from the anode to the cathode where the concentration of K^+ ions must be increased. With the anionic exchange ions (OH^-) of the Amberlyst A-26(OH) resin being identical to those anions in the electrolyte, the exchange of ions will not affect the flow cell performance by altering the electrolyte.

Using the same anode-to-cathode flow regime, it was hypothesized that using a strongly acidic ion exchange resin in the separating section between the electrodes would have a negative impact on flow cell performance. A strong acidic cation exchange resin, such as Amberlite IR-120H, would provide a reservoir of cations (H^+) in the separating section where the electrolyte Already needs a reduction of K+ ions to lower its concentration to match the OH- concentration and would not help with flow cell performance. There would be an exchange of H^+ ions from the Amberlite IR-120H resin with the K^+ ions from the electrolyte. The H^+ ions migrating into solution would react

with the OH^- ions present to produce water. Water formation consumes OH^- ions; preventing them from participating in the electrochemical reactions and dilutes the electrolyte. The electrolyte concentration is important because it is the driving force for the boundary layer diffusion of OH^- ions to the surface of solid active materials. It is important to note that the electrolyte solution would not be continually stripped of OH^- ions as to render it completely void of them because the interaction of the strongly acidic cation exchange material and the basic electrolyte solution would be constrained by equilibrium[71].

As seen in Figure 7.4, the flow cell performance obtained using the strongly acidic Amberlite IR-120H ion exchange resin as separating material was better than using stainless steel shot but not as good as using the strongly basic Amberlyst A-26(OH). It was thought that the parasitic nature of the strongly acidic resin on the basic electrolyte would result in flow cell performance worse than that obtained using a neutral stainless steel shot. This was most likely due to minimal electrolyte degradation due to favorable equilibrium conditions between the Amberlite IR-120H and the potassium hydroxide electrolyte.

Based on the results of using acidic and basic ion exchange resins as separating materials in the flow cell it was decided to examine the use of an ALL-CRAFT activated carbon as the separating material in the flow cell. Activated carbons are known to contain both acidic and basic reactive sites[72]. Activated carbons are used as catalyst

supports in packed-bed reactors and thus were not expected to pose a problem when used inside of the packed-bed flow cell.

It can be seen in Figure 7.4, that the use of ALL-CRAFT 4K activated carbon as the separating material averaged a 40 mV increase in operating cell potential over the use of Amberlyst A-26(OH) at the end of a 30-minute discharge through a 550-ohm resistive load. ALL-CRAFT activated carbons are chemically activated using potassium hydroxide as the activating agent. Although the carbons are washed thoroughly after activation it is possible that the activation with potassium hydroxide imparts basic sites in the carbon's surface structure.

It has been determined that a basic material exhibits better performance than an acidic material when used as a separating material in the flow cell. There could be a few reasons for the improved performance of the ALL-CRAFT 4K activated carbon over the Amberlyst A-26(OH) ion exchange resin. The manufacturing steps of the 4K activated carbon could provide stronger basic sites than those of the Amberlyst A-26(OH). If the basicity of the materials is similar then it could be the increased specific surface area of the smaller particle 4K activated carbon that allows for better base site utilization and thus better performance.

A rough estimation of the particle size of the 4K activated carbon was determined by passing the material through a set of sieves. Amberlyst A-26(OH) particles were then crushed using a mortar and pestle until visual comparison revealed particles similar in size to the 4K activated carbon. The crushed Amberlyst A-26(OH)

particles were then passed through the same set of sieves and the material collected from same sieves where the carbon had been constrained was used in a flow cell to evaluate performance. A comparison of the flow cell performance between the ALL-CRAFT 4K activated carbon, stock Amberlyst A-26(OH), and reduced particle size Amberlyst A-26(OH) is shown in Figure 7.5. The ALL-CRAFT 4K activated carbon performed better and the similar sized small particle Amberlyst A-26(OH) performed worse than the stock Amberlyst A-26(OH), so particle size can be ruled out as a reason for the performance gain of the 4K activated carbon.

The flow cell performance results shown in Figures 7.4 and 7.5 suggest that the ALL-CRAFT 4K activated carbon benefits flow cell performance by exhibiting a higher basicity than the Amberlyst A-26(OH). The basicity may be inherent in the material structure or it could be a product of electrolyte uptake into the pores of the activated carbon by way of absorption that acts as an electrolyte reservoir. The present work does not determine by what mechanism the activated carbon provides better flow cell performance, only that it does provide better performance by providing increased basicity.

7.5.2 Impact of Separation Distance in Presence of Separation Materials

In previous work it was determined that, in the absence of a separating material, flow cell performance decreased with an increase in the separation distance between the anode and cathode[69]. It is ideal to operate the flow cell with a minimum of a few centimeters of separation between the anode and cathode to dramatically reduce the

possibility of an internal short circuit failure. In an effort to compensate for the reduced performance at greater separation distances a look into flow cell performance at various separation distances in the presence of separation materials was conducted.

Figure 7.6 shows the performance of flow cells using Amberlyst A-26(OH) and stainless steel shot separation materials. Each material was evaluated in the flow cell with separation distances of 2.2-, 2.8-, 4.1-, and 5.4-cm between the electrodes. Based on flow cell performance shown in Figure 7.4, it was assumed that using stainless steel shot as the separation material would have lower performance than using the Amberlyst A-26(OH) and this remained true. In keeping with the same separation material, there is still a reduction in flow cell performance at increasing separation distances, but it is important to note that the Amberlyst A-26(OH) exhibited a much tighter range in performance between separation distances of 2.2-cm and 5.4-cm. There is about a 35 mV range in final voltage measurements between 2.2-cm and 5.4-cm of separation using Amberlyst A-26(OH). This is a 56% reduction from the 80 mV range between 2.2-cm and 5.4-cm of separation using stainless steel shot. The major improvement in flow cell performance associated with using Amberlyst A-26(OH) at 5.4-cm of separation between electrodes as opposed to using stainless steel shot at only 2.2-cm of separation indicates that the use of separation materials that interact positively with the electrolyte allow the cell to be operated with sufficiently large separation distances with minimal performance losses compared to using a separation material that does not ionically interact with the electrolyte.

7.5.3 Impact of Electrolyte Flow Direction

The impact of electrolyte flow direction on the flow cell was determined by circulating the electrolyte in an anode-to-cathode flow regime and then in a cathode-to-anode flow regime in the presence of both acidic (Amberlite IR-120H) and basic (Amberlyst A-26(OH)) ion exchange resins. It was hypothesized that the flow direction would have a dramatic impact on the flow cell performance because of possible differences in mechanisms needed to balance the electrolyte charges. It is believed than an acidic ion exchange resin used as a separating material would perform better than a basic ion exchange resin in the case of the electrolyte having increased concentrations of OH^- by aiding the K^+ ions in maintaining electrolyte charge balance. For a similar reason it is believed that use of a basic ion exchange resin as the separating material would perform better with electrolyte flowing from the anode to the cathode, as there would be a decrease in OH^- ions and a requirement of less K^+ ions in the electrolyte to balance charges, so the basic resin could occupy extra K^+ ions.The flow cell voltage profiles using both Amberlite IR-120H and Amberlyst A-26(OH) as separating materials with both electrolyte flow directions are shown in Figure 7.7. The flow cell performance using Amberlite IR-120H for the separating material is represented by the lower group of voltage profiles, while the flow cell results using Amberlyst A-26(OH) are shown in the higher group of voltage profiles. The solid lines show flow cell results obtained with electrolyte flowing from the anode to the cathode, and the dotted lines are results obtained with electrolyte flowing from cathode to anode.

As shown in Figure 7.7, the Amberlite IR-120H voltage profiles show only marginal performance gains associated with circulating the electrolyte from the cathode to the anode as opposed to anode-to-cathode circulation with a resistive load of 550-ohms applied to the flow cell. The increased OH^- ion concentration requires an increase in the K+ ion concentration and the acidic Amberlite IR-120H helps the K+ transfer from the anode where its mass needs to be reduced to the cathode where an increase in K+ ions are needed. It would be expected that increasing the discharge rate would result in a greater differences in flow cell performance associated with the 2 electrolyte flow directions. An increase in the discharge rate is analogous to either consuming (at anode) or producing (at cathode) OH^- ions faster, thus creating a larger challenge for charge balancing mechanisms in the electrolyte between the electrodes.

Figure 7.7 also shows that there were also small performance gains associated with circulating electrolyte from the cathode to the anode (increase in OH- and K+ concentrations) through the basic Amberlyst A-26(OH) resin. This is contrary to what was believed would happen, as with the basic resin it was hypothesized that it would occupy K^+ ions in the electrolyte and prevent an increase in K+ ion concentration at the cathode by intercepting K^+ ions being transferred to the cathode. This contradiction indicates the possibility that discharging through 550-ohms may produce too slow of a discharge rate to determine a discernable difference in flow cell performance between the 2 different flow regimes and that the marginal improvement discussed above for the Amberlite IR-120H may not be large enough to be deemed significant. A faster discharge rate would make the ionic imbalance between the electrodes larger. The lack

of complete dependence of performance on the direction of electrolyte flow may indicate a further dependency on electrolyte concentration and flow velocity.

7.6 Conclusions

A survey of materials used in the separating section between the electrodes of a packed-bed flow cell revealed that materials with basic properties outperform acidic and neutral materials. An interesting discovery was that an ALL-CRAFT 4K activated outperformed the strongly basic Amberlyst A-26(OH) when used as separating material in the flow cell. Particle size was ruled out as a reason for the 4K activated carbon success as similar size particles of 4K activated carbon and Amberlyst A-26(OH) resulted in voltage profiles above and below the voltage profile of stock Amberlyst A-26(OH), respectively.

A previous study indicated that an increase in the separation distance between the electrodes reduced the flow cell voltage. The present evaluation demonstrated that certain separator materials substantially reduce the loss in voltage associated increasing separation distances.

Although expected to make a difference at higher discharge rates, electrolyte flow direction had minimal impact while discharging through a 550-ohm load. It is expected for high discharge rate applications that the electrolyte flow direction will be an important factor to obtain optimal flow cell performance.

7.7 Acknowledgements

A special thanks is extended to the National Science Foundation (Award 0940720) for their generous financial support.

7.8 List of Figures

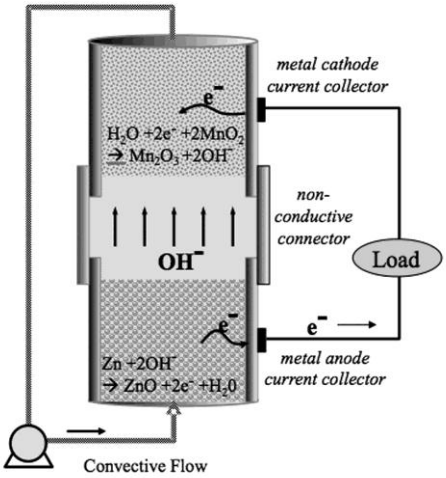

Figure 7.1. Schematic of flow cell with packed bed electrodes.

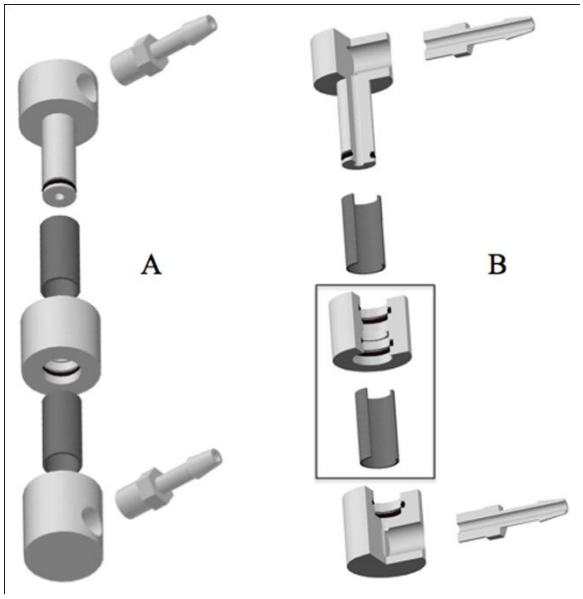

Figure 7.2. (a) 3-D image of packed-bed electrode flow cell, (b) Cutaway of packed-bed electrode flow cell, parts in box are repeated to expand flow cell for use of granular separation material.

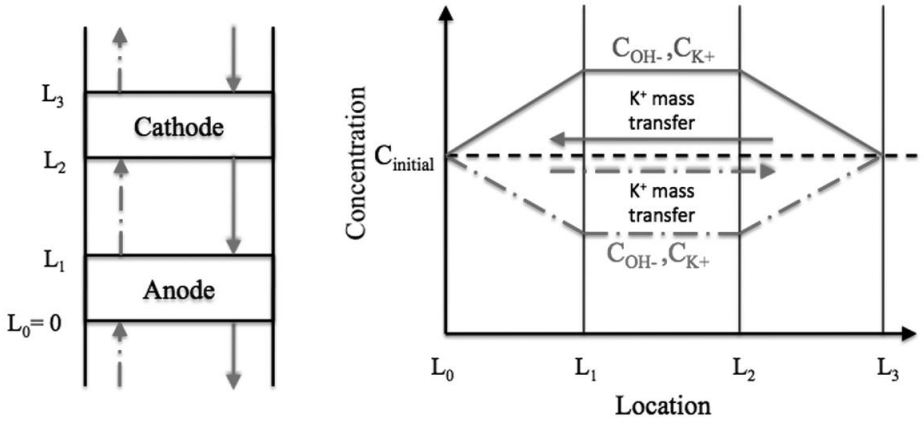

Figure 7.3. Electrolyte flow direction impact on electrolyte ion concentration profile, dash-dot line corresponds to anode-to-cathode flow and solid line corresponds to cathode-to-anode flow.

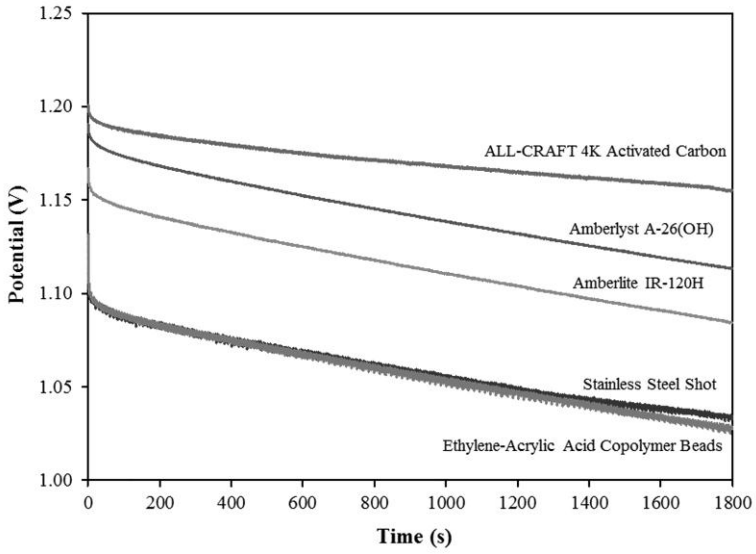

Figure 7.4. Average voltage profiles for packed-bed electrode flow cell with varied separation material.

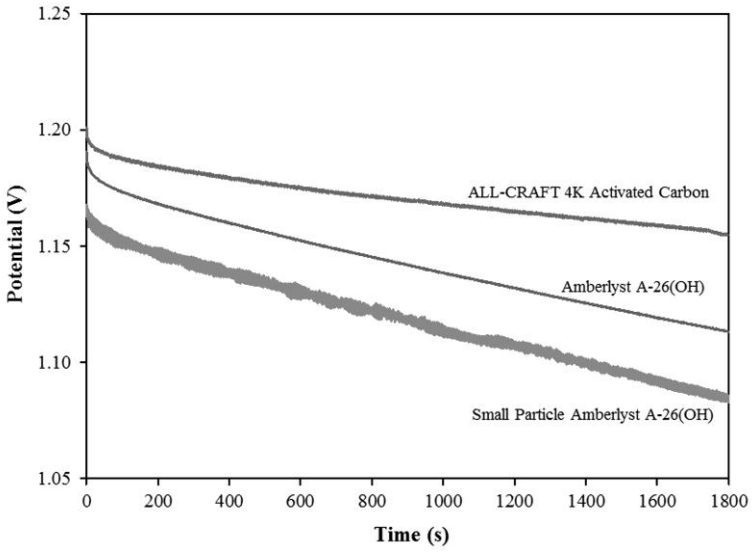

Figure 7.5. Average voltage profiles for packed-bed electrode flow cell comparing similar particle size ALL-CRAFT 4K activated carbon and small particle Amberlyst A-26(OH) to original Amberlyst A-26(OH).

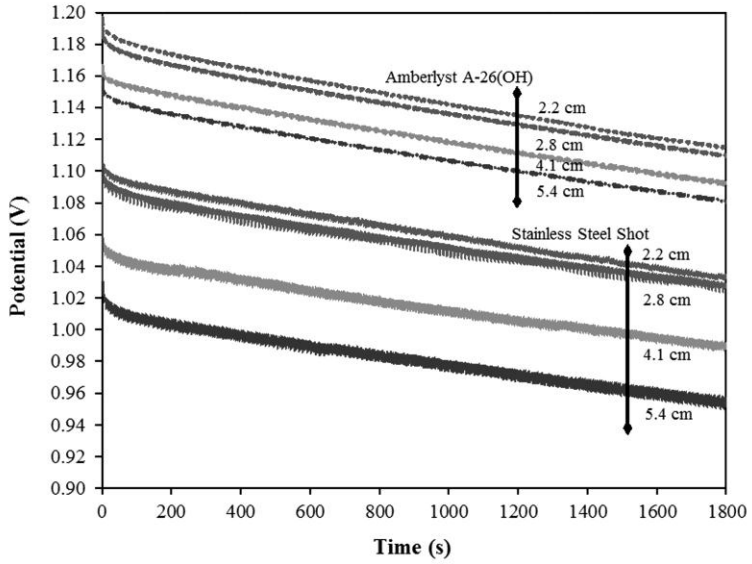

Figure 7.6. Voltage profiles for packed-bed electrode flow cell using 2 different separation materials, each at 4 different separation distances.

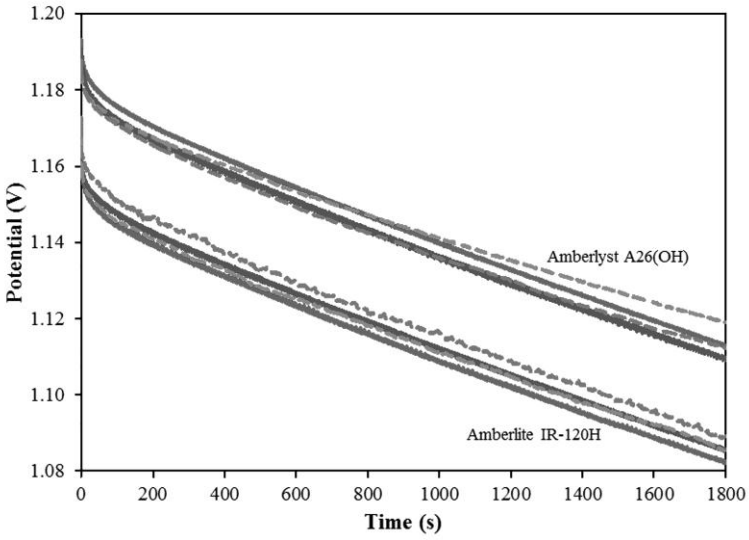

Figure 7.7. Voltage profiles for packed-bed electrode flow cell using an acidic and basic ion exchange resin as separation material, solid lines were obtained with an anode-to-cathode flow regime and dashed lines were obtained with a cathode-to-anode flow regime.

CHAPTER 8. CONCLUSIONS & RECOMMENDATIONS

As liquid fossil fuel resources become increasingly scarce, electrical energy will need to fill the increasing energy voids. The conventional technologies for electrical energy production are well established and renewable production of electrical energy is on the rise. It is important that electrical energy production be paired with efficient large-scale storage devices to maximize the potential of those energy production technologies. Current established flow battery technologies were developed for remote power system energy storage. Their relatively low specific energy (Wh kg^{-1}) is irrelevant for stationary electrical energy storage.

Hybrid electric vehicles currently employ conventional diffusion-based batteries as their specific energy significantly surpasses current established flow battery technologies. Vast research on redox flow batteries has greatly improved their specific energies since their conception, but soluble active materials will never be able to surpass the specific energies of solid-phase active materials. Flow battery specific energies must be improved before they can be applied to automotive applications and a transition to new flow battery technology may be the key.

The hybrid flow battery was a step in the right direction, as it eliminated the use of difficult and expensive separation membranes, eliminated the need for pumping a second electrolyte, and began using solid-phase active materials. A continued drawback of the hybrid flow battery is that it still uses parallel planar electrodes. Planar electrodes

are not space efficient. A planar electrode with large surface area requires a battery with at least one large dimension.

The research presented in this dissertation has proposed and validated the use of three-dimensional, packed-bed electrodes in a novel flow battery architecture. This type of flow battery mixes features of conventional diffusion-based batteries with the benefits of high reaction surface area to volume packed-bed electrodes and flowing electrolyte solutions. Large available surface area and electrolyte flow allow the packed-bed electrode flow battery to achieve higher energy densities by using solid active materials. The large surface area provides for a lower current density which aids in uniform deposition/dissolution of negative active materials. The electrolyte flow also helps to provide uniform deposition/dissolution by maintaining a uniform reaction ion concentration in solution.

It was determined by the research in this dissertation that the use of vertically stacked packed-bed electrodes requires the circulation of electrolyte through the battery to prevent voltage losses associated with reactive ion transport. The electrolyte flow is able to deliver reactive ions much faster than the diffusion only mechanisms used in conventional diffusion-based batteries and will therefore excel in situations of high-rate discharge of electrical current from the cell. In these high-rate discharge situations the flowing electrolyte can also be used for thermal management by flowing the electrolyte through a heat exchanger.

An increase in the separation distance between electrodes, from micrometer scales of diffusion-based batteries to centimeter scales in the packed-bed electrode flow battery, is desired as to prevent any chance of a dendrite induced short-circuit. The research in this dissertation found that increasing the electrode separation distance had a negative impact on the packed-bed electrode flow battery performance. The increasing voltage loss was attributed to an increasing resistance to the charge balancing efforts of the K+ counter-ion in the electrolyte solution. It was hypothesized that the addition of ionically active materials between the electrodes would reduce the voltage losses associated with electrode separation by aiding in the charge balancing of the electrolyte. Initial improved performance was obtained by using an anion exchange resin, Amberlyst A-26(OH), between the electrodes as opposed to using relatively non-ionically active stainless steel. This discovery led to a survey of materials used for the separating material of the packed-bed electrode flow battery and an activated carbon, ALL-CRAFT 4K, outperformed all materials surveyed including the Amberlyst A-26(OH).

It is important to make sure net energy can be harvested from a flow battery that requires a pump to circulate the electrolyte. Using a basis of a 2 kWh (7200 kJ) zinc/alkaline/manganese dioxide battery operating at 1.2V using 2M KOH with a 2 atmosphere packed-bed pressure drop being discharge at 2 amps until complete reaction of the active materials is obtained, 20.94 kJ of energy (assuming a pump efficiency of 30%) is required to pump the stoichiometric amount of electrolyte. This 20.94 kJ of energy is 0.291% of the 7200 kJ of energy supplied by the battery. (See Appendix for calculations) These calculations indicates that net energy can be expected

from packed-bed electrode flow batteries despite having to circulate electrolyte through the battery.

This validation of the use of packed-bed electrodes in a flow battery has great potential for the improvement of flow battery technology. These improvements in flow battery technology are needed before the flow battery can be applied to vehicle technology. The results of this initial packed-bed electrode flow battery study indicate that the design it is worthy of further study.

REFERENCES

1. Brown, T. L.; Lemay, H.E.; Bursten, B. E. *Chemistry: The Central Science*. 8th ed.; Prentice Hall: Upper Saddle River, NJ, 2000; p 1024.

2. Linden, D., Basic Concepts. In *Handbook of Batteries*, 3rd ed.; Linden, D.; Reddy, T., Eds. McGraw-Hill: Chicago, 2002; p 1200.

3. (a) Aurbach, D.; Zinigrad, E.; Cohen, Y.; Teller, H. A short review of failure mechanisms of lithium metal and lithiated graphite anodes in liquid electrolyte solutions. *Solid State Ionics* **2002,** *148* (3,4), 405-416; (b) Mori, M.; Naruoka, Y.; Naoi, K.; Fauteux, D. Modification of the lithium metal surface by nonionic polyether surfactants: quartz crystal microbalance studies. *Journal of the Electrochemical Society* **1998,** *145* (7), 2340-2348.

4. Suppes, G. J. Convection battery configuration for connective carbon matrix electrode. 2009-US62991, 2010051540, 20091102., 2010.

5. Cairns, E. J.; Albertus, P., Batteries for electric and hybrid-electric vehicles. *Annual Review of Chemical and Biomolecular Engineering* **2010,** *1*, 299-320.

6. Wald, M., California regulators to meet on electric cars. *New York Times* [Online] 1994, May 12, http://www.nytimes.com/1994/05/12/business/california-regulators-to-meet-on-electric-cars.html (accessed October 5, 2010).

7. Adelson, A., G.M. tries to increase appeal of electric car. *New York Times* [Online] 1998, December 18, http://www.nytimes.com/1998/12/18/automobiles/gm-tries-to-increase-appeal-of-electric-car.html (accessed October 5, 2010).

8. Taylor III, A. The Birth of the Prius. http://money.cnn.com/magazines/fortune/fortune_archive/2006/03/06/8370702/ (accessed October 5, 2010).

9. Taniguchi, A.; Fujioka, N.; Ikoma, M.; Ohta, A. Development of nickel/metal-hydride batteries for EVs and HEVs. *Journal of Power Sources* **2001,** *100* (1-2), 117-124.

10. Tesla About Tesla. http://www.teslamotors.com/about (accessed October 5, 2010).

11. Zhang, L. Y. Rare earth based metal hydrides and NiMH rechargeable batteries. *Rare Earths: Science, Technology & Applications III, held during the TMS Annual Meeting, Orlando, Fla., Feb. 9-13, 1997* **1997**, 235-257.

12. Linden, D.; Magnusen, D., Portable Sealed Nickel-Metal Hydride Batteries. In *Handbook of Batteries*, 3rd ed.; Linden, D.; Reddy, T., Eds. McGraw-Hill: Chicago, 2002; p 1200.

13. Nagaura, T.; Tozawa, K. Lithium ion rechargeable battery. *Progress in Batteries & Solar Cells* **1990,** *9*, 209-17.

14. Patoux, S.; Daniel, L.; Bourbon, C.; Lignier, H.; Pagano, C.; Le Cras, F.; Jouanneau, S.; Martinet, S. High voltage spinel oxides for Li-ion batteries: From the material research to the application. *Journal of Power Sources* **2009,** *189* (1), 344-352.

15. Ozawa, K. Lithium-ion rechargeable batteries with LiCoO2 and carbon electrodes: the LiCoO2/C system. *Solid State Ionics* **1994,** *69* (3-4), 212-21.

16. (a) Kim, D.-H.; Kim, J. Synthesis of LiFePO4 Nanoparticles in Polyol Medium and Their Electrochemical Properties. *Electrochemical and Solid-State Letters* **2006,** *9* (9), A439-A442; (b) Lee, J.; Teja, A. S. Synthesis of LiFePO4 micro and nanoparticles in supercritical water. *Materials Letters* **2006,** *60* (17-18), 2105-2109; (c) Prosini, P. P.; Carewska, M.; Scaccia, S.; Wisniewski, P.; Pasquali, M. Long-term cyclability of nanostructured LiFePO4. *Electrochimica Acta* **2003,** *48* (28), 4205-4211; (d) Sides, C. R.; Croce, F.; Young, V. Y.; Martin, C. R.; Scrosati, B. A High-Rate, Nanocomposite LiFePO4/Carbon Cathode. *Electrochemical and Solid-State Letters* **2005,** *8* (9), A484-A487.

17. (a) Shin, H. C.; Cho, W. I.; Jang, H. Electrochemical properties of the carbon-coated LiFePO4 as a cathode material for lithium-ion secondary batteries. *Journal of Power Sources* **2006,** *159* (2), 1383-1388; (b) Wang, G. X.; Needham, S.; Yao, J.; Wang, J. Z.; Liu, R. S.; Liu, H. K. A study on LiFePO4 and its doped derivatives as cathode materials for lithium-ion batteries. *Journal of Power Sources* **2006,** *159* (1), 282-286; (c) Yang, M.-R.; Ke, W.-h.; Wu, S.-h. Improving electrochemical properties of lithium iron phosphate by addition of vanadium. *Journal of Power Sources* **2007,** *165* (2), 646-650.

18. Jiang, J.; Dahn, J. R. ARC studies of the thermal stability of three different cathode materials: LiCoO2; Li[Ni0.1Co0.8Mn0.1]O2; and LiFePO4, in LiPF6 and LiBoB EC/DEC electrolytes. *Electrochemistry Communications* **2004,** *6* (1), 39-43.

19. Tesla Battery. http://www.teslamotors.com/roadster/technology/battery (accessed October 5, 2010).

20. Ohnsman, A. Toyota Remains With Nickel After Lithium Prius Test (Update3). http://www.bloomberg.com/apps/news?pid=newsarchive&sid=aI7Ov7Jyo2nU (accessed October 5, 2010).

21. Toyota Prius Plug-In Hybrid. http://www.toyota.com/upcoming-vehicles/prius-plug-in/technology.html (accessed October 5, 2010).

22. Ehrlich, G. M., Lithium-Ion Batteries. In *Handbook of Batteries*, Third Edition ed.; Linden, D.; Reddy, T., Eds. McGraw-Hill: Chicago, 2002; p 1200.

23. (a) Barbarich, T. J.; Gnanaraj, J. S.; DiCarlo, J. Low temperature electrolytes for lithium-ion batteries. *Proceedings of the Power Sources Conference* **2006,** *42nd*, 257-260; (b) Luo, H.-j.; Zhang, X.-g., BMIPF6 as high temperature additive in LiPF6-based lithium ion electrolytes. *Dianyuan Jishu* **2009,** *33* (10), 873-875.

24. (a) Smart, M. C.; Smith, K. A.; Bugga, R. V.; Prakash, S. G.; Krause, F. C. Lithium-ion electrolytes containing flame retardant additives for increased safety characteristics. 2009-543495, 2010047695, 20090818., 2010; (b) Xu, K.; Ding, M. S.; Zhang, S.; Allen, J. L.; Jow, T. R. An attempt to formulate nonflammable lithium ion electrolytes with alkyl phosphates and phosphazenes. *Journal of the Electrochemical Society* **2002,** *149* (5), A622-A626.

25. Spotnitz, R.; Franklin, J. Abuse behavior of high-power, lithium-ion cells. *Journal of Power Sources* **2003,** *113* (1), 81-100.

26. Berdichevsky, G.; Kelty, K.; Straubel, J.; Toomre, E. The Tesla Roadster Battery System. http://www.teslamotors.com/display_data/TeslaRoadsterBatterySystem.pdf (accessed October 19, 2010).

27. Gaines, L. *Costs of Lithium-Ion Batteries for Vehicles*; Argonne National Laboratory: Argonne, Illinois, May, 2000.

28. United States Advanced Battery Consortium. Development of Advanced High-Performance Batteries for Plug-In Electric Vehicle Applications. http://www.uscar.org/commands/files_download.php?files_id=118 (accessed October 19, 2010).

29. Thaller, L. H. Electrically rechargeable redox flow cells. *Intersoc. Energy Convers. Eng. Conf. Proc., 9th* **1974**, 924-8.

30. Rychcik, M.; Skyllas-Kazacos, M. Characteristics of a new all-vanadium redox flow battery. *Journal of Power Sources* **1988,** *22* (1), 59-67.

31. Hagedorn, N. H.; Thaller, L. H. Redox storage systems for solar applications. *Power Sources* **1981,** *8*, 227-43.

32. Thaller, L. H. Recent advances in Redox flow cell storage systems. *Proceedings of the Intersociety Energy Conversion Engineering Conference* **1979,** *14th* (Vol. 1), 715-21.

33. Lopez-Atalaya, M.; Codina, G.; Perez, J. R.; Vazquez, J. L.; Aldaz, A. Optimization studies on an iron/chromium redox flow battery. *Journal of Power Sources* **1992,** *39* (2), 147-54.

34. Alexander, S. S.; Hodgdon, R. B.; Waite, W. A. *Anion permselective membrane*; Res. Div.,Ionics, Inc.,Watertown,MA,USA.: 1979; p 52 pp.

35. Nozaki, K.; Ozawa, T. ETL 1 kW redox flow cell. *Progress in Batteries & Solar Cells* **1984,** *5*, 327-30.

36. Earley, J. E.; Cannon, R. D. Aqueous chemistry of chromium(III). *Transition Metal Chem.* **1965,** *1*, 33-109.

37. Reid, M. A.; Thaller, L. H. Improvement and scale-up of the NASA redox storage system. *Proceedings of the Intersociety Energy Conversion Engineering Conference* **1980,** *15th* (2), 1471-6.

38. Giner, J. D.; Cahill, K. J. Catalyst surfaces for the chromous/chromic redox couple. 79-61555, 61555, 19790727., 1980.

39. Gahn, R. F.; Charleston, J.; Ling, J. S.; Reid, M. A. *Performance of advanced chromium electrodes for the NASA Redox Energy Storage System*; Lewis Res. Cent.,NASA,Cleveland,OH,USA.: 1981; p 23 pp.

40. Skyllas-Kazacos, M.; Rychcik, M.; Robins, R. G.; Fane, A. G.; Green, M. A. New all-vanadium redox flow cell. *Journal of the Electrochemical Society* **1986,** *133* (5), 1057-8.

41. Sukkar, T.; Skyllas-Kazacos, M. Modification of membranes using polyelectrolytes to improve water transfer properties in the vanadium redox battery. *Journal of Membrane Science* **2003,** *222* (1-2), 249-264.

42. Mohammadi, T.; Skyllas Kazacos, M. Modification of anion-exchange membranes for vanadium redox flow battery applications. *Journal of Power Sources* **1996,** *63* (2), 179-186.

43. Zeng, J.; Jiang, C.; Wang, Y.; Chen, J.; Zhu, S.; Zhao, B.; Wang, R. Studies on polypyrrole modified nafion membrane for vanadium redox flow battery. *Electrochemistry Communications* **2008,** *10* (3), 372-375.

44. Kim, J.-G.; Lee, S.-H.; Choi, S.-I.; Jin, C.-S.; Kim, J.-C.; Ryu, C.-H.; Hwang, G.-J. Application of Psf-PPSS-TPA composite membrane in the all-vanadium redox flow battery. *Journal of Industrial and Engineering Chemistry (Amsterdam, Netherlands)* **2010,** *16* (5), 756-762.

45. Chen, D.; Wang, S.; Xiao, M.; Han, D.; Meng, Y. Sulfonated poly(fluorenyl ether ketone) membrane with embedded silica rich layer and enhanced proton selectivity for vanadium redox flow battery. *Journal of Power Sources* **2010,** *195* (22), 7701-7708.

46. Rychcik, M.; Skyllas-Kazacos, M. Evaluation of electrode materials for vanadium redox cell. *Journal of Power Sources* **1987,** *19* (1), 45-54.

47. Skyllas-Kazacos, M. Novel vanadium chloride/polyhalide redox flow battery. *Journal of Power Sources* **2003,** *124* (1), 299-302.

48. Sum, E.; Rychcik, M.; Skyllas-Kazacos, M. Investigation of the vanadium(V)/vanadium(IV) system for use in the positive half-cell of a redox battery. *Journal of Power Sources* **1985,** *16* (2), 85-95.

49. Skyllas-Kazacos, M.; Kazacos, G.; Poon, G.; Verseema, H. Recent advances with UNSW vanadium-based redox flow batteries. *International Journal of Energy Research* **2010,** *34* (2), 182-189.

50. Hazza, A.; Pletcher, D.; Wills, R. A novel flow battery: A lead acid battery based on an electrolyte with soluble lead(II). Part I. Preliminary studies. *Physical Chemistry Chemical Physics* **2004,** *6* (8), 1773-1778.

51. Pletcher, D.; Wills, R. A novel flow battery - A lead acid battery based on an electrolyte with soluble lead(II): III. The influence of conditions on battery performance. *Journal of Power Sources* **2005,** *149*, 96-102.

52. Li, X.; Pletcher, D.; Walsh, F. C. A novel flow battery: A lead acid battery based on an electrolyte with soluble lead(II): Part VII. Further studies of the lead dioxide positive electrode. *Electrochimica Acta* **2009,** *54* (20), 4688-4695.

53. Cheng, J.; Zhang, L.; Yang, Y.-S.; Wen, Y.-H.; Cao, G.-P.; Wang, X.-D. Preliminary study of single flow zinc-nickel battery. *Electrochemistry Communications* **2007,** *9* (11), 2639-2642.

54. Zhang, L.; Cheng, J.; Yang, Y.-s.; Wen, Y.-h.; Wang, X.-d.; Cao, G.-p. Study of zinc electrodes for single flow zinc/nickel battery application. *Journal of Power Sources* **2008,** *179* (1), 381-387.

55. Cheng, J.; Wen, Y.-H.; Cao, G.-P.; Yang, Y.-S. Influence of zinc ions in electrolytes on the stability of nickel oxide electrodes for single flow zinc-nickel batteries. *Journal of Power Sources* **2011,** *196* (3), 1589-1592.

56. Tessier, C.; Faure, C.; Guerlou-Demourgues, L.; Denage, C.; Nabias, G.; Delmas, C. Electrochemical Study of Zinc-Substituted Nickel Hydroxide. *Journal of the Electrochemical Society* **2002,** *149* (9), A1136-A1145.

57. Pan, J.; Sun, Y.; Cheng, J.; Wen, Y.; Yang, Y.; Wan, P. Study on a new single flow acid Cu-PbO2 battery. *Electrochemistry Communications* **2008,** *10* (9), 1226-1229.

58. Kanamura, K.; Tamura, H.; Shiraishi, S.; Takehara, Z.-i. Morphology and chemical compositions of surface films of lithium deposited on a Ni substrate in nonaqueous electrolytes. *Journal of Electroanalytical Chemistry* **1995,** *394* (1-2), 49-62.

59. Kim, I.; Weil, R. An electron microscopy study of the initial stages of dendrite formation in electrodeposited zinc. *Surface Technology* **1985,** *25* (1), 1-6.

60. Geankoplis, C. J., *Transport Processes and Separation Process Principles*. 4th ed.; Prentice Hall: Upper Saddle River, NJ, 2003; p 1026.

61. Bird, R. B.; Stewart, W. E.; Lightfoot, E. N., *Transport Phenomena*. 2nd ed.; John Wiley & Sons, Inc.: New York, NY, 2002; p 895.

62. Zhang, S. S. A review on the separators of liquid electrolyte Li-ion batteries. *Journal of Power Sources* **2007,** *164* (1), 351-364.

63. Treptow, R. S. Lithium batteries: A practical application of chemical principles. *Journal of Chemical Education* **2003,** *80* (9), 1015-1020.

64. (a) Cheng, J.; Luo, X.; Yan, X.; Li, Z.; Tang, Y.; Jiang, H.; Zhu, W. Research progress in cation-pi interactions. *Science in China, Series B: Chemistry* **2008,** *51* (8), 709-717; (b) Radford, G. J. W.; Cox, J.; Wills, R. G. A.; Walsh, F. C. Electrochemical characterization of activated carbon particles used in redox flow battery electrodes. *Journal of Power Sources* **2008,** *185* (2), 1499-1504; (c) Wang, X.; Wang, Y.; Xue, F.; Li, J.; Liu, Y.; Wang, T.; Ye, F.; Miao, R. Integrated device of electrode tank and current collector for redox flow battery. 2008-20108417, 201204228, 20080530., 2009.

65. Puskar, M.; Harris, P. Reserve, flowing electrolyte, high rate lithium battery. *Proceedings of the International Power Sources Symposium* **1986,** *32nd*, 331-6.

66. Hart, T. G. Electrochemical System. 4,237,197, December 2, 1980.

67. Pan, J.; Ji, L.; Sun, Y.; Wan, P.; Cheng, J.; Yang, Y.; Fan, M. Preliminary study of alkaline single flowing Zn-O2 battery. *Electrochemistry Communications* **2009,** *11* (11), 2191-2194.

68. Zocchi, A. Redox Flow Battery and Method of Operating It. 6,692,862 B1, February 17, 2004.

69. Suppes, G. J.; Sawyer, B. D.; Gordon, M. J. High-Energy Density Flow Battery Validation. *AICHE Journal*, n/a, doi: 10.1002/aic.12390.

70. Pfeifer, P.; Suppes, G. J.; Shah, P.; Burress, J. W. Biomass-derived high surface area carbon materials with large micropores. 2007-US84061, 2008058231, 20071108., 2008.

71. De Lucas, A.; Zarca, J.; Canizares, P. Ion-exchange equilibrium of calcium, magnesium, potassium, sodium, and hydrogen ions on Amberlite IR-120: experimental determination and theoretical prediction of the ternary and quaternary equilibrium data. *Separation Science and Technology* **1992,** *27* (6), 823-41.

72. (a) Leon, C. A.; Leon, D.; Radovic, L. R. Interfacial chemistry and electrochemistry of carbon surfaces. *Chemistry and Physics of Carbon* **1994,** *24*, 213-310; (b) Lopez-Ramon, M. V.; Stoeckli, F.; Moreno-Castilla, C.; Carrasco-Marin, F., On the characterization of acidic and basic surface sites on carbons by various techniques. *Carbon* **1999,** *37* (8), 1215-1221.

APPENDIX

Pumping Energy Calculations

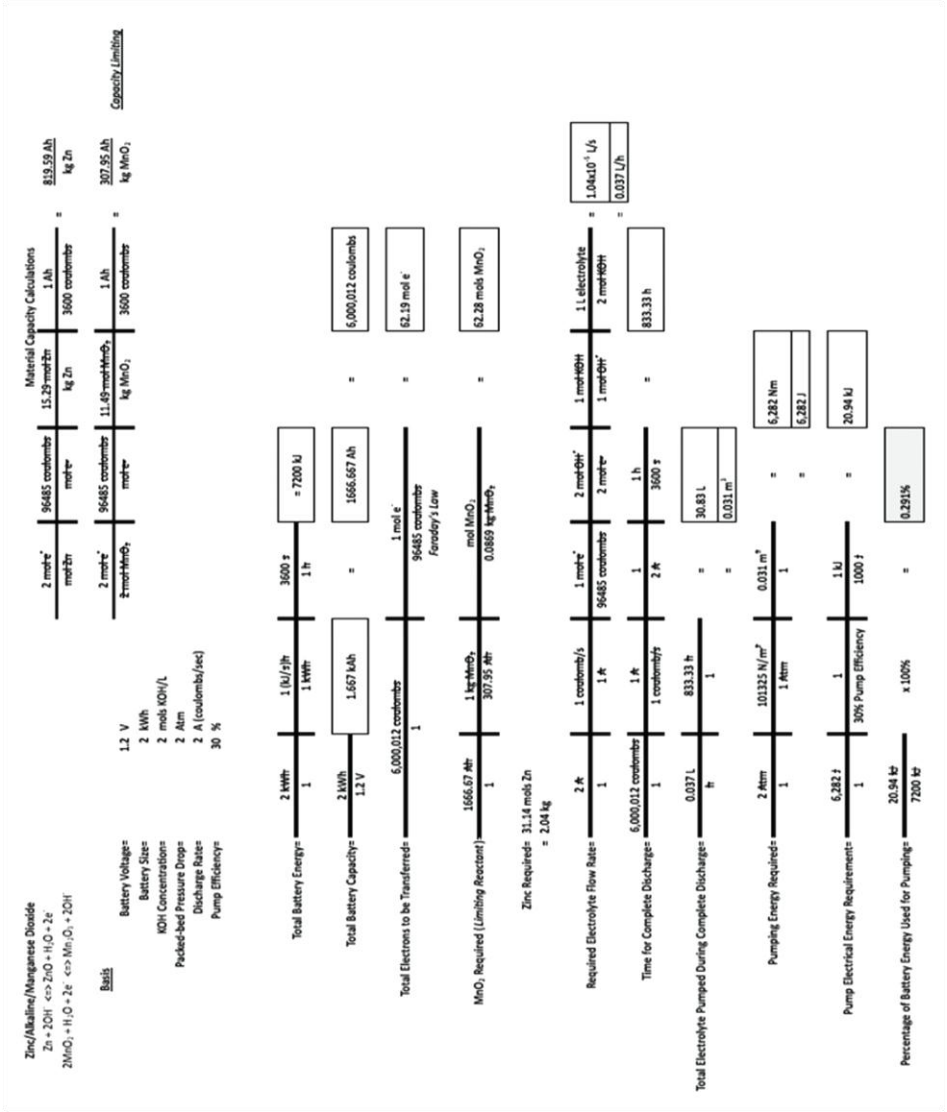

VITA

Bryan Dustin Sawyer was born October 6, 1982 in St. Joseph, Missouri. He earned his Bachelor of Science degree in Chemical Engineering from the University of Missouri in May 2006. He began graduate school at the University of Missouri in June 2006 and completed all requirements needed to earn a Doctor of Philosophy degree in Chemical Engineering in December 2010.